[1]J. D. Bjorken and S. D. Drell, *Relativistic Quantum Mechanics* (McGraw-Hill, New York, 1964), pp. 261–268.

[2]R. L. Garwin, L. M. Lederman, and M. Weinrich, Phys. Rev. **104**, 1415 (1957); J. I. Friedman and V. L. Telegdi, Phys. Rev. **106**, 1290 (1957); J. C. Sens, R. A. Swanson, V. L. Telegdi, and D. D. Yovanovitch, Phys. Rev. **107**, 1465 (1957).

[3]J. H. Brewer, K. M. Crowe, R. F. Johnson, A. Schenck, and R. W. Williams, Phys. Rev. Lett. **27**, 297 (1971).

[4]V. G. Nosov and I. V. Iakovleva, Zh. Eksp. Teor. Fiz. **43**, 1750 (1962) [Sov. Phys.-JETP **16**, 1236 (1963)].

[5]"Chemical shifts" in ω_μ due to diamagnetic shielding by atomic electrons are usually on the order of a few dozen ppm. These frequency shifts are measurable and could provide clues as to the final environment of the muons, but will be neglected in this treatment.

[6]I. G. Ivanter and V. P. Smilga, Zh. Eksp. Teor. Fiz. **54**, 559 (1968) [Sov. Phys.-JETP **27**, 301 (1968)].

[7]I. G. Ivanter and V. P. Smilga, Zh. Eksp. Teor. Fiz. **55**, 1521 (1968) [Sov. Phys.-JETP **28**, 796 (1969)].

[8]I. G. Ivanter, Zh. Eksp. Teor. Fiz. **56**, 1419 (1969) [Sov. Phys.-JETP **29**, 761 (1969)].

[9]I. G. Ivanter and V. P. Smilga, Zh. Eksp. Teor. Fiz. **60**, 1985 (1971) [Sov. Phys.-JETP **33**, 1070 (1971)]; I. G. Ivanter and V. P. Smilga, Zh. Eksp. Teor. Fiz. **61**, 2176 (1972) [Sov. Phys.-JETP **34**, 1167 (1972)].

[10]V. G. Firsov and V. M. Byakov, Zh. Eksp. Teor. Fiz.

[ ]47, 1074 (1964) [Sov. Phys.-JETP **20**, 719 (1965)]; V. G. Firsov, Zh. Eksp. Teor. Fiz. **48**, 1179 (1965) [Sov. Phys.-JETP **21**, 786 (1965)].

[11]A. I. Babaev, M. Ya. Balats, G. G. Myasishcheva, Yu. V. Obukhov, V. S. Roganov, and V. G. Firsov, Zh. Eksp. Teor. Fiz. **50**, 877 (1966) [Sov. Phys.-JETP **23**, 583 (1966)].

[12]J. H. Brewer, Ph. D. thesis (Lawrence Berkeley Laboratory Report No. LBL-950, 1972) (unpublished). Experimental results will be submitted for publication.

[13]K. M. Crowe, J. F. Hague, J. E. Rothberg, A. Schenck, D. L. Williams, R. W. Williams, and K. K. Young, Phys. Rev. A **5**, 2145 (1972).

[14]S. K. Allison and M. Garcia-Munoz, *Atomic and Molecular Processes*, edited by D. R. Bates (Academic, New York, 1962), Chap. 19; R. Wolfgang, Prog. React. Kinet. **3**, 99 (1965); F. S. Rowland, J. Am. Chem. Soc. **90**, 4767 (1968).

[15]R. K. Wangsness and F. Bloch, Phys. Rev. **89**, 728 (1953).

[16]P. Neta, R. W. Fessenden, and R. H. Schuler, 75, 1654 (1971). Typical relaxation rates for the electron of atomic hydrogen in liquids are evidently $<10^5\ sec^{-1}$.

[17]In the language of chemical kinetics, the reaction $Mu+X\to D$ is described by the second-order equation

$-d\,[Mu]/dt = -d\,[X]/dt = k_{mxd}\,[Mu]\,[X]$, where [Mu] should be interpreted as the probability of a Mu atom still being uncombined at some t. Since $[Mu]\le 1$, $[X]$ is constant, and the problem reduces to the first-order equation

$-d\,[Mu]/dt = \Lambda_{mxd}[Mu]$, where $\Lambda_{mxd}=k_{mxd}\,[X]$.

Muonium. IV. Precision Measurement of the Muonium Hyperfine-Structure Interval at Weak and Very Weak Magnetic Fields*

P. A. Thompson,† P. Crane,‡ T. Crane, J. J. Amato,§ V. W. Hughes, G. zu Putlitz,∥ and J. E. Rothberg**

Gibbs Laboratory, Physics Department, Yale University, New Haven, Connecticut 06520

(Received 18 December 1972)

A complete discussion is given of our precision measurement of the hyperfine-structure interval $\Delta\nu$ of the ground state of muonium at a weak magnetic field ($\sim$ 3 G) using the resolved transitions $(F, M_F) = (1, \pm 1) \to (0, 0)$, and at a very weak magnetic field ($\sim$ 10 mG) using unresolved transitions $\Delta F = \pm 1$. The method of magnetic resonance studies of muonium is used, where a single oscillatory field is employed and the resonance line is swept by varying the applied frequency. This research yielded values for the coefficients of the linear hfs density shifts for muonium in argon and krypton at a temperature of approximately 20 °C: $a_{M-Ar} = -5.00(22) \times 10^{-9}$/torr, $a_{M-Kr} = -10.57(39) \times 10^{-9}$/torr, and also for the quadratic hfs pressure-shift coefficients: $b_{M-Ar} = 8.1(2.5) \times 10^{-15}$/(torr)^2, $b_{M-Kr} = 8.6(5.9) \times 10^{-15}$/(torr)^2. The value obtained for $\Delta\nu$ is $\Delta\nu = 4463.308(11)$ MHz (2.5 ppm), where the 1-standard-deviation error is principally a statistical counting error. Our result for $\Delta\nu$ is in good agreement with other measurements of $\Delta\nu$ and also with the current theoretical value.

I. INTRODUCTION

This paper is the fourth paper in the series[1-3] of complete reports of research on muonium by the Yale group.[4] It gives a detailed discussion of our precision measurement of the hyperfine-structure interval $\Delta\nu$ of muonium through the observation of a magnetic resonance transition between hyperfine states at low magnetic field. A natural and common method[5,6] of determining the hyper- fine-structure interval of an atom by radio-frequency or microwave spectroscopy is to measure directly the transition frequency between the hfs levels at a low magnetic field, where the transition frequency is closely equal to the hfs interval $\Delta\nu$. The motivation for a precise determination of $\Delta\nu$, and the general theory and experimental method of magnetic resonance studies of muonium, have been discussed in the earlier papers of this series.

In the course of our precision measurement of $\Delta\nu$ at low magnetic field it was necessary to study carefully the dependence of $\Delta\nu$ on the gas pressure of argon and krypton. We determined both the linear and the quadratic coefficients of the dependence of $\Delta\nu$ on pressure.

The Chicago group has recently also measured $\Delta\nu$ at low magnetic field using the method of separated oscillating fields,[7] and has also reported values for the linear and quadratic coefficients of the hfs pressure shift.[8]

Section II of the present paper presents the theory of the experiment, including the energy levels and the resonance line shapes. Section III describes the experimental method and apparatus. Section IV presents the data analysis, and Sec. V gives our results and conclusions. Brief reports of this research have been published.[9-12]

II. THEORY OF EXPERIMENT

A. Energy Levels and Transition Frequencies

General expressions for the energy levels, eigenfunctions, and transition frequencies for muonium in a static magnetic field have been given in Muonium II.[2] We review these results here and specialize them to the case of low magnetic field. The general expression for the energy levels is

$$W_{F=1/2\pm1/2,\,M_F} = -\tfrac{1}{4}\Delta W + \mu_B^\mu g'_\mu M_F H$$

$$\pm\tfrac{1}{2}\Delta W(1 + 2M_F x + x^2)^{1/2}, \quad (2.1)$$

in which F is the total-angular-momentum quantum number; M_F is the associated magnetic quantum number; ΔW is the hfs interval between the $F=1$ and $F=0$ states ($\Delta W = h\Delta\nu$); $\mu_B^\mu = e\hbar/2m_\mu c$; m_μ is the muon mass; g'_μ is the muon gyromagnetic ratio in muonium; $\vec{H}$ is the external static magnetic field; $x = (g_J\mu_B^e - g'_\mu\mu_B^\mu)H/\Delta W$; g_J is the electron gyromangetic ratio in muonium; $\mu_B^e = e\hbar/2m_e c$; m_e is the electron mass.

At low field ($x \ll 1$) where only the terms linear in H need be retained, the energy levels $W_{F,\,M_F}$ reduce to

$$W_{1,1} = +\tfrac{1}{4}\Delta W + (g_J\mu_B^e + g'_\mu\mu_B^\mu)H/2\ ,$$

$$W_{1,0} = +\tfrac{1}{4}\Delta W\ ,$$

$$W_{1,-1} = +\tfrac{1}{4}\Delta W - (g_J\mu_B^e + g'_\mu\mu_B^\mu)H/2\ , \quad (2.2)$$

$$W_{0,0} = -\tfrac{3}{4}\Delta W\ .$$

Figure 1 gives a plot of these energy levels; for convenience the energy levels are numbered as indicated.

The corresponding transition frequencies at low magnetic field, which are of interest in the present paper, are

$$\nu_{14} = \Delta\nu + (g_J\mu_B^e + g'_\mu\mu_B^\mu)H/2h\ ,$$

$$\nu_{24} = \Delta\nu\ , \quad (2.3)$$

$$\nu_{34} = \Delta\nu - (g_J\mu_B^e + g'_\mu\mu_B^\mu)H/2h\ .$$

Clearly at sufficiently low magnetic field these transition frequencies are approximately equal to the hfs interval $\Delta\nu$.

B. Theory of Resonance Line Shape

As for the case of our experiments at strong magnetic field, transitions are induced between the hfs magnetic substates of muonium by application of a microwave magnetic field. The associated time-dependent Hamiltonian term is given by

$$\mathcal{H}'(t) = (g_J\mu_B^e\vec{J} + g'_\mu\mu_B^\mu\vec{I}_\mu)\cdot\vec{H}_1\cos\omega t$$

$$= \mathcal{H}'_0\cos\omega t\ , \quad (2.4)$$

in which $\vec{H}_1$ is the vector amplitude of the applied microwave field, ω is its angular frequency, $\vec{J}$ is the electronic angular momentum operator, and $\vec{I}_\mu$ is the muon-spin operator.

Two types of transitions have been utilized. In the first only two levels are involved in the resonance transition, and the other levels are off resonance. This type of transition, designated a weak-field transition, is obtained at a magnetic
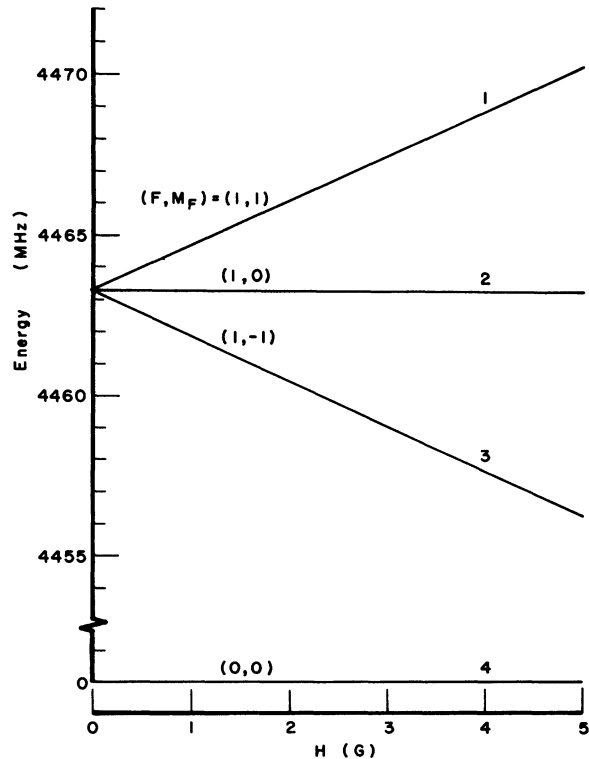

FIG. 1. Energy-level diagram for muonium in its ground state at low magnetic field as given by Eq. (2.2).

field which is weak (e.g., ~3 G) but still large
enough so that the three transition frequencies ν_{14},
ν_{24}, and ν_{34} differ by frequencies large compared
to the resonance linewidths. The second type of
transition, designated a very-weak-field transi-
tion, involves three or four levels in the resonance
transition. It is obtained at very weak magnetic
field (e.g., 10 mG) at which the three transition
frequencies ν_{14}, ν_{24}, and ν_{34} are not resolved.

1. Weak-Field Transition

The theory of the resonance line shape for the
two-level case has been treated in detail in Muoni-
um II[2] and Muonium III,[3] and the results are essen-
tially applicable to a weak-field transition. Equa-
tions (2.10) and (2.12) of Muonium III give the
state probabilities for the two-level case, which
can be applied to the weak-field transitions ν_{14} or
ν_{34}. Hence for the transition ν_{14}, with the inclu-
sion of the off-resonant states 2 and 3, we obtain,
as in Eq. (2.16) of Muonium III, the differential
time-integrated signal $dS(\theta)$. This is the nor-
malized difference between the numbers of detected
decay positrons emitted in the direction θ, with
respect to the direction of the weak field, $\vec{H} = H\hat{k}$,
with the microwave power on and off:

$$dS(\theta) = a\cos\theta\, LK, \qquad (2.5)$$

in which

$$K = \frac{[(\chi_1^* | 2I_{\mu z}|\chi_1) - (\chi_4^* | 2I_{\mu z}|\chi_4)][\,|a_4(0)|^2 - |a_1(0)|^2]}{(e^{-\gamma t_1} - e^{-\gamma t_2})[1 + a\cos\theta\sum_{i=1}^{4}|a_i(0)|^2(\chi_i^*|2I_{\mu z}|\chi_i)]} \qquad (2.5a)$$

and

$$L = \frac{2|b|^2}{\Gamma^2}\left[e^{-\gamma t_1}\left(1 - g(t_1)\frac{\gamma^2}{\Gamma^2 + \gamma^2}\right)\right.$$
$$\left. - e^{-\gamma t_2}\left(1 - g(t_2)\frac{\gamma^2}{\Gamma^2 + \gamma^2}\right)\right], \qquad (2.5b)$$

where

$$g(t) = \cos\Gamma t - (\Gamma/\gamma)\sin\Gamma t$$

and χ_i ($i = 1, 2, 3, 4$) is the spin eigenfunction for
muonium[1] in state i; $a_i(t)$ ($i = 1, 2, 3, 4$) is the am-
plitude of muonium state i at time t; $I_{\mu z}$ is the
operator for the z component of muon spin; γ is
the muon decay rate; a is the asymmetry factor
associated with muon decay [Eq. (2.7b) of Muoni-
um III]; (t_1, t_2) is the time interval after muonium
formation, taken as time $t = 0$, during which decay
positrons are observed; $b = b_{14} = (\chi_1^*|\mathcal{H}_0'|\chi_4)/2\hbar$;
$\Gamma^2 = \omega'^2 + 4|b|^2$; $\omega' = \omega_{14} - \omega$, in which $\omega_{14} = 2\pi\nu_{14}$.
The formula for the matrix element b is given in
Table I of Muonium II. Formulas for the forma-
tion probabilities of the muonium states are given

in Eq. (3.11) of Muonium I. Equation (2.5) ne-
glects the off-resonance frequency component
$e^{+i\omega t}$ (or $e^{-i\omega t}$) in the microwave magnetic field.
Furthermore, it is a differential signal since it re-
fers to a small volume in the microwave cavity
over which the microwave field $\vec{H}_1$ is constant and
to an infinitesimal size detector. The same ex-
pression holds for the transition ν_{34} with the sub-
stitution of 3 for 1 throughout. A general expres-
sion for the total signal S involves integration over
the target volume and detector area. Furthermore,
the expression for S which is fitted to the observa-
tional data has a normalization constant. [See
Eq. (2.19) and associated discussion in Muonium
III.[3]]

For the time interval $(t_1, t_2) = (0, \infty)$, Eq. (2.5b)
for L gives the Lorentzian line shape:

$$L = \frac{2|b|^2}{\Gamma^2 + \gamma^2}. \qquad (2.6)$$

It is useful to note several differences between
the transition ν_{12} at strong field discussed in Mu-
onium II and III and the weak-field transitions ν_{14}
and ν_{34} of interest in the present paper. At weak
field the hfs interaction in muonium plays an im-
portant role in determining the initial-state popu-
lations, and indeed for $x \ll 1$, which is the case of
interest here, these probabilities are

$$|a_1(0)|^2 = \tfrac{1}{2}, \quad |a_2(0)|^2 = \tfrac{1}{4},$$
$$|a_3(0)|^2 = 0, \quad |a_4(0)|^2 = \tfrac{1}{4} \qquad (2.7)$$

for completely polarized incident muons with M_μ
$= +\tfrac{1}{2}$. Hence for the transition ν_{14} (ν_{34}), the factor
$|a_4(0)|^2 - |a_1(0)|^2$ [$|a_4(0)|^2 - |a_3(0)|^2$], which ap-
pears in K[Eq. (2.5a)] and is proportional to the
signal intensity, equals $-\tfrac{1}{4}$ ($+\tfrac{1}{4}$), whereas the cor-
responding factor for the strong-field case is $-\tfrac{1}{2}$.
{Note that for Eq. (2.16) for Muonium III the nor-
malization of the state probabilities is different
[Eq. (2.9) of Muonium III].} In addition, the factor
$[(\chi_1^*|2I_{\mu z}|\chi_1) - (\chi_4^*|2I_{\mu z}|\chi_4)]$, which appears in K
and is also proportional to the signal intensity, has
the value $+\tfrac{1}{2}$ ($-\tfrac{1}{2}$) for the ν_{14} (ν_{34}) transition,
whereas the corresponding factor for the strong-
field case is 1. Hence owing to these two factors
the signal intensity for the weak-field transition is
$\tfrac{1}{4}$ that of the strong-field transition.

Another outstanding difference between the
strong-field and weak-field transitions is the much
larger magnitude of the quantity $|b|/H_1$ for the
weak-field transition as compared to the strong-
field transition. This difference occurs because
the weak-field transitions are allowed transitions
caused primarily by the time-dependent interac-
tion term in $\mathcal{H}'(t)$ of Eq. (2.4) which involves g_J,
whereas the strong-field transition is a "forbidden"

transition which is also caused primarily by this g_J interaction term.

For the weak-field transition ν_{14}, the presence of the nonresonant state 3 and of the matrix element b_{34} (see Table I of Muonium II) leads to a shift in the resonance frequency[13]:

$$(\delta\omega)_{14} = (\omega_{34} - \omega_{14}) \frac{|b_{34}|^2}{(\omega_{34} - \omega_{14})^2} . \qquad (2.8)$$

For the conditions of our experiment, $(\delta\omega)_{14} \lesssim 0.2$ ppm.

$$\begin{pmatrix} \dot{a}_1 \\ \dot{a}_2 \\ \dot{a}_3 \\ \dot{a}_4 \end{pmatrix} = \begin{pmatrix} -\gamma/2 & 0 & 0 & -ib_{14}e^{+i(\omega_{14}-\omega)t} \\ 0 & -\gamma/2 & 0 & 0 \\ 0 & 0 & -\gamma/2 & -ib_{34}e^{+i(\omega_{34}-\omega)t} \\ -ib_{14}^* e^{-i(\omega_{14}-\omega)t} & 0 & -ib_{34}^* e^{-i(\omega_{34}-\omega)t} & -\gamma/2 \end{pmatrix} \begin{pmatrix} a_1 \\ a_2 \\ a_3 \\ a_4 \end{pmatrix} . \qquad (2.9)$$

Clearly the coupled equations involve the three states 1, 3, and 4 only.

a. Transition at zero field. For the special case of $H = 0$, the relations $\omega_{14} = \omega_{34} = 2\pi\Delta\nu (\equiv \omega_0)$ and $b_{14} = -b_{34}^* = b$ hold. In this case the three coupled equations can be reduced to an equivalent two-lev-

$$\begin{pmatrix} \dot{A}_+ \\ \dot{A}_- \\ \dot{a}_4 \end{pmatrix} = \begin{pmatrix} -\gamma/2 & 0 & 0 \\ 0 & -\gamma/2 & -i\sqrt{2}\,be^{i(\omega_0-\omega)t} \\ 0 & -i\sqrt{2}\,be^{-i(\omega_0-\omega)t} & -\gamma/2 \end{pmatrix} \begin{pmatrix} A_+ \\ A_- \\ a_4 \end{pmatrix} . \qquad (2.11)$$

Only the state amplitudes A_- and a_4 are coupled, so we have a two-level problem. Solution for the state amplitudes in terms of the initial (complex) values $a_1(0)$, $a_3(0)$, and $a_4(0)$ gives

$$A_+(t) = \left(\frac{a_1(0) + a_3(0)}{\sqrt{2}}\right) e^{-\gamma t/2} ,$$

$$A_-(t) = \left\{ \left(\frac{a_1(0) - a_3(0)}{\sqrt{2}}\right) \left[\cos\frac{\Gamma_0 t}{2} - \frac{i\omega'}{\Gamma_0} \sin\frac{\Gamma_0 t}{2}\right] \right.$$

$$\left. + a_4(0) \left[-\frac{i2\sqrt{2}\,b}{\Gamma_0} \sin\frac{\Gamma_0 t}{2}\right] \right\} e^{-\gamma t/2 + i\omega' t/2} ,$$

$$\qquad (2.12)$$

$$a_4(t) = \left\{ \left(\frac{a_1(0) - a_3(0)}{\sqrt{2}}\right) \left[\frac{-i2\sqrt{2}\,b}{\Gamma_0} \sin\frac{\Gamma_0 t}{2}\right] \right.$$

$$\left. + a_4(0) \left[\cos\frac{\Gamma_0 t}{2} + \frac{i\omega'}{\Gamma_0} \sin\frac{\Gamma_0 t}{2}\right] \right\} e^{-\gamma t/2 - i\omega' t/2} ,$$

in which

$$\omega' = \omega_0 - \omega \quad \text{and} \quad \Gamma_0 = (\omega'^2 + 8|b|^2)^{1/2} . \qquad (2.12a)$$

2. Very-Weak-Field Transition

For the very-weak-field case[14,15] all four states must in general be considered. The z axis is chosen parallel to $\vec{H}$ and we assume that $\vec{H}_1$ is perpendicular to $\vec{H}$; hence there are no nonzero matrix elements with $\Delta M_F = 0$. We neglect matrix elements which oscillate rapidly compared to the muon decay rate γ. The time-dependent coupled equations for the state amplitudes can be written in matrix form:

el problem. If we choose the x axis parallel to $\vec{H}_1$, then the state amplitudes A_+ and A_-, defined by the linear combinations

$$A_+ = \tfrac{1}{2}\sqrt{2}\,(a_1 + a_3) , \quad A_- = \tfrac{1}{2}\sqrt{2}\,(a_1 - a_3) , \qquad (2.10)$$

satisfy the matrix equations

The state amplitudes $a_1(t)$ and $a_3(t)$ are then given by

$$a_1(t) = \tfrac{1}{2}\sqrt{2}\,[A_+(t) + A_-(t)] ,$$

$$a_3(t) = \tfrac{1}{2}\sqrt{2}\,[A_+(t) - A_-(t)] . \qquad (2.13)$$

In the observation of a resonance line the relevant quantity is the z component of muon polarization in the muonium state Ψ:

$$P_z(t) = P_{z0}(t)e^{-\gamma t} = \langle\Psi^*| 2I_{\mu z} |\Psi\rangle$$

$$= \sum_{i,j=1}^{4} a_i^* a_j \langle\chi_i^*| 2I_{\mu z} |\chi_j\rangle e^{i\omega_{ij}t} , \qquad (2.14)$$

in which

$$\Psi = \phi(\vec{r}) \sum_{i=1}^{4} a_i \chi_i e^{-iW_i t/\hbar} \qquad (2.14a)$$

as in Eq. (2.2a) of Muonium III[3] and the χ_i are the usual zero-field spin eigenfunctions as given in Muonium I.[1] At zero field we obtain

$$P_z(t) = |a_1|^2 - |a_3|^2 + a_2^* a_4 e^{i\omega_{24}t} + a_4^* a_2 e^{-i\omega_{24}t} .$$
$$(2.15)$$

Since the muon decay rate γ is very small compared to the resonance frequency ω_{24}, the cross-product terms can be neglected. Hence we obtain

$$P_z(t) = |a_1(t)|^2 - |a_3(t)|^2 = 2\,\mathrm{Re}[A_+^*(t)A_-(t)] , \quad (2.16)$$

and, using Eq. (2.12),

$$P_z(t) = 2\,\mathrm{Re}\left\{ A_+^*(0)e^{-\gamma t + i\omega' t/2} \right.$$

$$\times \left[A_-(0)\left(\cos\frac{\Gamma_0 t}{2} - \frac{i\omega'}{\Gamma_0}\sin\frac{\Gamma_0 t}{2} \right) \right.$$

$$\left.\left. + a_4(0)\left(\frac{-i\,2\sqrt{2}\,b}{\Gamma_0}\sin\frac{\Gamma_0 t}{2} \right) \right] \right\} . \quad (2.17)$$

If the above analysis leading to Eq. (2.17) is redone using for the time dependence of the microwave magnetic field in Eq. (2.4) the factor $\cos(\omega t + \phi)$ rather than $\cos\omega t$, the only change in Eq. (2.17) is the replacement of b by $be^{i\phi}$. To obtain the resonance line shape corresponding to an ensemble of muons, we must average over ϕ and, hence, the term linear in b will not contribute to the line shape. Hence equation (2.17) can be taken to be

$$P_z(t) = 2\,\mathrm{Re}\left\{ A_+^*(0)e^{-\gamma t + i\omega' t/2} \right.$$

$$\left. \times \left[A_-(0)\left(\cos\frac{\Gamma_0 t}{2} - \frac{i\omega'}{\Gamma_0}\sin\frac{\Gamma_0 t}{2} \right) \right] \right\} .$$

$$(2.18)$$

In order to proceed further we need to have expressions for the initial-state amplitudes $a_1(0)$ and $a_3(0)$.

The proper treatment of the line-shape theory requires the use of the density matrix[16] for muonium since we are dealing with an ensemble of muonium atoms. It is convenient to introduce this density matrix at this point in the discussion. We assume that the incident muons have a polarization P in the z direction and that the atomic electrons are unpolarized. The density matrices for the muons and for the electrons are[17]

$$\rho_\mu = \frac{1}{2}\begin{pmatrix} 1+P & 0 \\ 0 & 1-P \end{pmatrix} , \quad \rho_e = \frac{1}{2}\begin{pmatrix} 1 & 0 \\ 0 & 1 \end{pmatrix} . \quad (2.19)$$

Hence calculation of the combined muon and electron, or muonium, density matrix ρ yields

$$\rho(0) = \frac{1}{4}\begin{pmatrix} 1+P & 0 & 0 & 0 \\ 0 & 1 & 0 & +P \\ 0 & 0 & 1-P & 0 \\ 0 & +P & 0 & 1 \end{pmatrix} . \quad (2.20)$$

The symbol $\rho(0)$ is the density matrix ρ at time $t = 0$. The matrix element is $\rho_{ij}(0) = \langle a_i^*(0)a_j(0)\rangle$, where the ensemble average is indicated and $a_i(0)$ and $a_j(0)$ are the amplitudes of the zero-magnetic-field eigenstates [Eq. (2.4) of Muonium I] in the wave function for an atom in the ensemble.

Evaluation of the muonium ensemble average of P_z for Eq. (2.18) yields

$$\langle P_z(t)\rangle = \frac{1}{4}Pe^{-\gamma t}\left[\left(\frac{\Gamma_0 + \omega'}{\Gamma_0} \right)\cos\left(\frac{\Gamma_0 - \omega'}{2} \right)t \right.$$

$$\left. + \left(\frac{\Gamma_0 - \omega'}{\Gamma_0} \right)\cos\left(\frac{\Gamma_0 + \omega'}{2} \right)t \right] . \quad (2.21)$$

We remark that the step from Eq. (2.17) to Eq. (2.18) can also be validated from the density matrix $\rho(0)$ for the ensemble since the density matrix elements ρ_{14} and ρ_{34} equal zero. The calculation of the signal requires the evaluation of $\int_{t_1}^{t_2} \langle P_z(t)\rangle\,dt$ over the observation time interval (t_1, t_2). If we choose the interval $(t_1, t_2) = (0, \infty)$, we obtain

$$\int_0^\infty \gamma\langle P_z(t)\rangle\,dt = \frac{P}{2}\frac{\gamma^2(\gamma^2 + \omega'^2 + 2|b|^2)}{(\gamma^2 + 2|b|^2)^2 + \omega'^2\gamma^2} .$$

$$(2.22)$$

We follow the approach in Sec. II of Muonium III and calculate the difference ΔN between the number of positrons emitted with the microwave magnetic field on and with the microwave magnetic field off, normalized for a single muon:

$$\Delta N(y_0, \theta, t_1 = 0, t_2 = \infty) = \left(\frac{d\Omega\cos\theta\,A_2(y_0)}{4\pi} \right)\left(\frac{P}{2} \right)$$

$$\times \left(\frac{-2|b|^2(\gamma^2 + 2|b|^2)}{(\gamma^2 + 2|b|^2)^2 + \omega'^2\gamma^2} \right) , \quad (2.23)$$

in which y_0 is the minimum positron momentum detected in units of $m_\mu c/2$ and θ is the polar angle with respect to the z axis. The function $A_2(y_0)$ is given by

$$A_2(y_0) = \frac{1}{3} - (y_0^4 - \frac{2}{3}y_0^3) . \quad (2.24)$$

The differential signal $dS(\theta)$ is

$$dS(\theta) = \frac{\Delta N(y_0, \theta, t_1 = 0, t_2 = \infty)}{N^0(y_0, \theta, t_1 = 0, t_2 = \infty)} , \quad (2.25)$$

in which $N^0(y_0, \theta, t_1 = 0, t_2 = \infty)$ is the number of decay positrons observed with the microwave power off:

$$N^0(y_0, \theta, t_1 = 0, t_2 = \infty) = (d\Omega/4\pi)A_1(y_0)[1 + \frac{1}{2}aP\cos\theta] ,$$

$$(2.26)$$

where

$$A_1(y_0) = 1 - (2y_0^3 - y_0^4) . \quad (2.26a)$$

Hence using Eqs. (2.23)–(2.26), the quantity $dS(\theta)$ takes the form

$$dS(\theta) = a\cos\theta\, L'K' \ , \tag{2.27}$$

in which

$$a(y_0) = A_2(y_0)/A_1(y_0) \ , \tag{2.27a}$$

$$L' = \frac{-2|b|^2(\gamma^2 + 2|b|^2)}{(\gamma^2 + 2|b|^2)^2 + \omega'^2\gamma^2} \ , \tag{2.27b}$$

$$K' = \frac{\tfrac{1}{2}P}{1 + \tfrac{1}{2}aP\cos\theta} \ . \tag{2.27c}$$

To obtain a general expression for the total signal S we must integrate Eq. (2.27) over the volume in which muons are stopped and over the finite size of the detector, taking into account the distribution and polarization of stopped muons in the gas and in the walls, the fraction of muons forming muonium, and the microwave magnetic field in the resonant cavity used. The expression given for S in Eq. (2.28) takes into account only muons stopping in the gas within the microwave cavity and is based on the assumption that all these muons form muonium:

$$S = \mathfrak{K}'\int_V \rho aL'(\int_D \cos\theta\, d\Omega)\, d\tau \ , \tag{2.28}$$

in which L' is given in Eq. (2.27b). $\mathfrak{K}'$ is given by

$$\mathfrak{K}' = \frac{\tfrac{1}{2}P}{\int_V \rho[\int_D(1 + \tfrac{1}{2}aP\cos\theta)d\Omega]d\tau} \ , \tag{2.28a}$$

where V is the active volume of the microwave cavity in which muonium is formed, D is the positron-detector area, $d\Omega$ is the differential solid

angle subtended by an element of the detector area at a point in the volume, and ρ is the density distribution of stopped muons. Equation (2.28) is used for the analysis of our resonance curves and the quantity $\mathfrak{K}'$ is treated as a parameter to be determined in the data analysis. This analysis procedure should be valid for our objectives (see Sec. IV) and is necessitated because of our lack of detailed knowledge of the muon density distribution, background counts, muon polarization, and muonium formation.

Several features of the resonance line shape for the three-level zero-field case can be ascertained by consideration of the expression for L' of Eq. (2.27b). At resonance L' becomes

$$L'(\omega' = 0) = \frac{-2|b|^2}{\gamma^2 + 2|b|^2} \ . \tag{2.29}$$

For comparison the corresponding quantity for the two-level weak-field signal is

$$L(\omega' = 0) = \frac{2|b|^2}{\gamma^2 + 4|b|^2}$$

[Eq. (2.6)]. Hence for the three-level case the signal saturates at a higher value of $|b|^2$. From Eq. (2.27b) we find that the full width at half-maximum intensity is given by

$$\delta\nu_{12} = \frac{\gamma^2 + 2|b|^2}{\pi\gamma} \ . \tag{2.30}$$

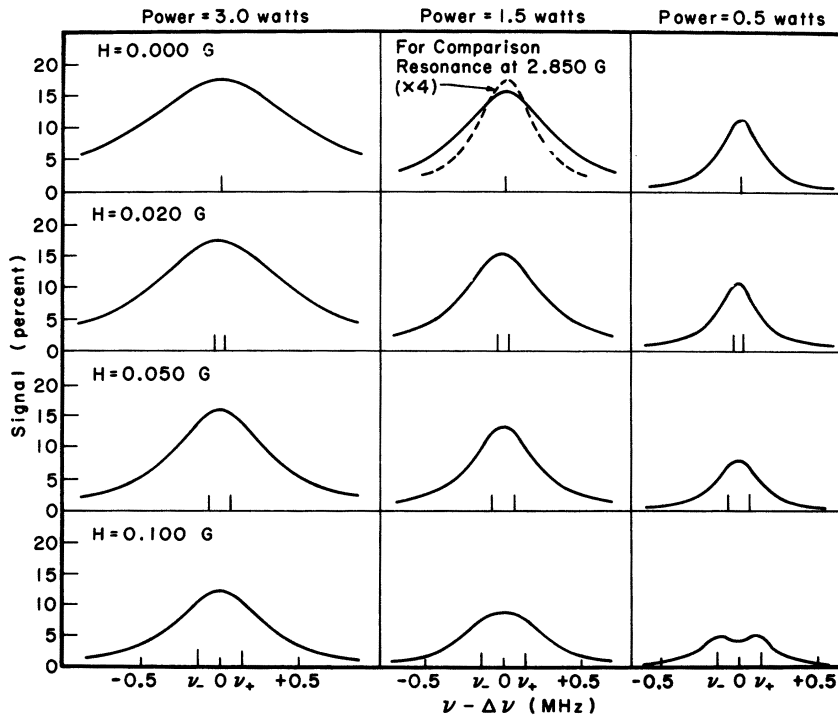The natural width, obtained in the limit of zero

FIG. 2. Calculated line shapes for transitions at very weak magnetic field for several values of magnetic field H and input microwave power P to a cavity with $Q = 14\,000$ and operating in the TM_{220} mode. The percent signal is plotted vs the difference between the applied microwave frequency ν and the hfs interval $\Delta\nu$. The quantities ν_+ and ν_- equal $\nu_{14} - \Delta\nu$ and $\nu_{34} - \Delta\nu$, respectively. The comparison resonance signal at 2.850 G is plotted versus $\nu - \nu_{14}$.
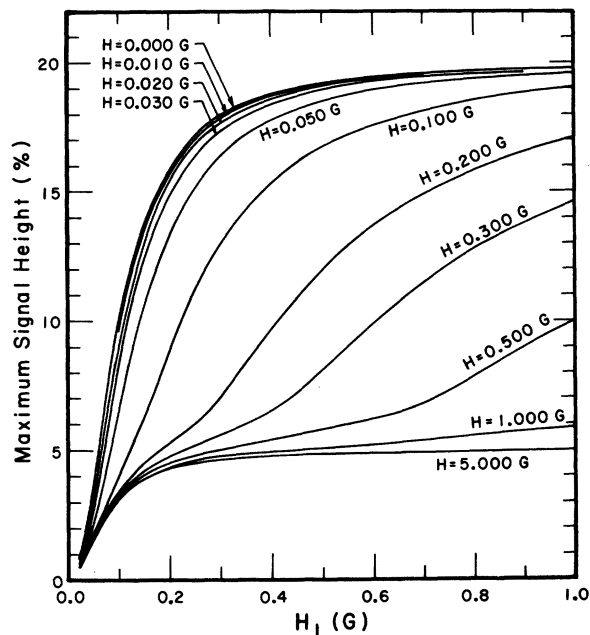
FIG. 3. Calculated maximum signal height vs micro-
wave magnetic field strength H_1 at several low magnetic
fields H. Equation (A16) is used to determine the height
with the constant parameters chosen as $a = \frac{1}{3}$, $\cos\theta = -1$,
and $P = 1$.

microwave power, is γ/π, as it is for the two-lev-
el case [Eq. (2.6)]. However, the broadening of
the line in the three-level zero-field case is pro-
portional to the microwave power or $|b|^2$ at high
power, whereas in the two-level case the broaden-
ing is proportional to the square root of the micro-
wave power [Eq. (2.29), Muonium II].

b. Transition at nonzero field. In a very weak
but nonzero magnetic field H, the resonance line
shape must be obtained from a solution of Eq.
(2.9). One method of solution is given in the Ap-
pendix. Solutions to Eq. (2.9) were also obtained
via computer techniques to eliminate some of the
tedious algebra, and this approach is also dis-
cussed in the Appendix. Information available from
our solutions of Eq. (2.9) is given in Figs. 2–4 and
in Tables I and II.

The principal conclusions from the results of the
nonzero-field solution for $H < 20$ mG are the follow-
ing: (i) The line shape is approximately Lorentz-
ian and reduces smoothly to the zero-field line
shape as H is reduced to zero (see Fig. 2 and Ta-
ble I). (ii) The maximum signal intensity is close
to that at zero field (see Figs. 2 and 3 and Table I).
(iii) The linewidth is slightly less than the zero-
field value and has approximately the same depen-
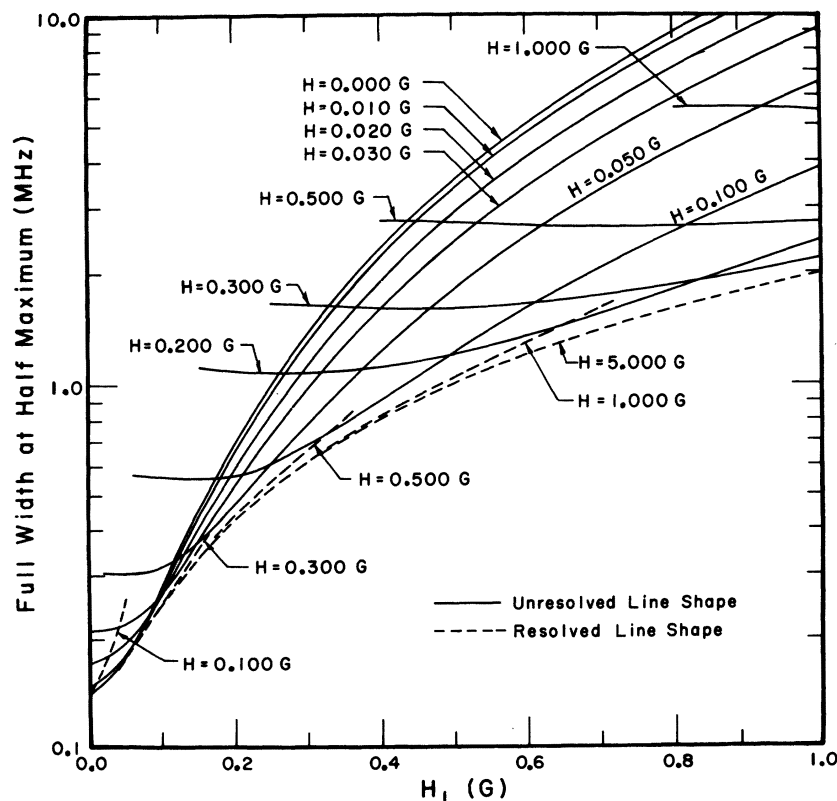dence on microwave field strength (see Figs. 2 and

FIG. 4. Calculated linewidth
(full width at half-maximum) vs
microwave magnetic field strength
H_1 at several low magnetic fields
H. The line shapes are considered
resolved if the signal height for
any microwave frequency between
ν_{34} and ν_{14} is less than half the
signal height at ν_{14} or ν_{34}. As H_1
is increased, the linewidth is con-
sidered to double when the line
shape changes from a resolved
transition to an unresolved transi-
tion.

TABLE I. Results of the analytic solution [Eq. (A16)] for percent signal as a function of microwave frequency ν at very weak magnetic field H. The microwave magnetic field is chosen to be $H_1 = 0.161$ G (see Sec. IIID). The other parameters in Eq. (A16) were given the values: $a = \frac{1}{3}$, $\cos\theta = -1$, and $P = 1$.

$(\nu - \Delta\nu)$ (KHz)	H (mG)									
	0	1	2	3	5	10	20	50	100	200
0	14.232	14.230	14.226	14.218	14.194	14.081	13.646	11.223	6.867	2.690
50	13.688	13.686	13.680	13.670	13.639	13.497	12.974	10.575	6.881	2.803
100	12.280	12.277	12.267	12.254	12.208	12.002	11.304	8.976	6.732	3.146
150	10.483	10.480	10.468	10.450	10.391	10.132	9.306	7.115	6.111	3.700
200	8.701	8.697	8.684	8.664	8.599	8.318	7.460	5.476	5.079	4.339
250	7.140	7.136	7.123	7.103	7.039	6.762	5.944	4.204	3.985	4.738
300	5.856	5.852	5.840	5.821	5.761	5.503	4.761	3.265	3.066	4.561
350	4.830	4.826	4.815	4.798	4.743	4.511	3.854	2.579	2.370	3.876
400	4.017	4.014	4.004	3.989	3.940	3.734	3.160	2.074	1.861	3.053
450	3.374	3.371	3.363	3.349	3.306	3.124	2.624	1.696	1.488	2.343

4 and Table I). (iv) The line center equals the hfs interval $\Delta\nu$ to within the accuracy of the calculation. This result is to be expected because the quadratic Zeeman effect is negligibly small for all the energy levels and the linear Zeeman effect for the levels $(F, M_F) = (1,1)$ and $(1, -1)$ at 20 mG has a magnitude of 28 kHz and is of opposite sign for the two levels.

The slight deviations of the signal height and width from the zero-field case of Eq. (2.27b) can be taken into account for the very-weak-field case with $H < 20$ mG by fitting analytic expressions to computer-generated solutions of Eq. (2.9) for the signal intensity and the linewidth as a function of magnetic field H and microwave field strength H_1. An adequate fit is given by the Lorentzian expression

TABLE II. Comparison of two-level solution [Eq. (2.5)] and three-level solution [Eq. (A16)] for percent signal for the transition ν_{14}, $(F, M_F) = (1, 1) \longleftarrow (0, 0)$, at weak magnetic field. The microwave magnetic field is chosen to be $H_1 = 0.228$ G (see Sec. IIID). The other parameters in the equations were given the values: $a = \frac{1}{3}$, $\cos\theta = -1$, and $P = 1$.

$(\nu - \nu_{14})$ (kHz)	$H = 1.0$ G		$H = 3.0$ G		$H = 5.0$ G	
	3-level	2-level	3-level	2-level	3-level	2-level
500	0.856	0.841	0.839	0.840	0.837	0.838
450	1.008	0.995	0.992	0.993	0.990	0.992
400	1.200	1.190	1.185	1.188	1.184	1.186
350	1.445	1.439	1.432	1.436	1.430	1.434
300	1.768	1.757	1.747	1.754	1.746	1.751
250	2.156	2.161	2.148	2.157	2.147	2.153
200	2.652	2.663	2.646	2.658	2.644	2.653
150	3.235	3.250	3.229	3.243	3.227	3.236
100	3.847	3.857	3.836	3.848	3.831	3.840
50	4.355	4.344	4.327	4.333	4.318	4.323
0	4.580	4.535	4.529	4.524	4.513	4.513
−50	4.425	4.344	4.349	4.333	4.332	4.323
−100	3.959	3.857	3.871	3.848	3.852	3.840
−150	3.356	3.250	3.267	3.243	3.249	3.236
−200	2.763	2.663	2.679	2.658	2.664	2.653
−250	2.253	2.161	2.176	2.157	2.163	2.153
−300	1.840	1.757	1.769	1.754	1.759	1.751
−350	1.515	1.439	1.449	1.436	1.441	1.434
−400	1.262	1.190	1.199	1.188	1.192	1.186
−450	1.063	0.995	1.003	0.993	0.997	0.992
−500	0.907	0.841	0.848	0.840	0.843	0.838

$$L''(H) = \frac{-2|b|^2}{\gamma^2 + 2|b|^2 + C_1 H} \left[\frac{w^2}{4\pi^2(\nu - \nu_0)^2 + w^2} \right], \quad (2.31)$$

$$w(H) = [\gamma^2 + 2|b|^2(1 - C_2 H)]/\gamma, \quad (2.31a)$$

where $C_1 = 5$ MHz^2 G^{-1}, $C_2 = 6.5$ G^{-1}, ν is the applied frequency, and ν_0 is the frequency of the line center. These expressions are valid for $H \leqslant 0.020$ G and $H_1 \leqslant 0.5$ G, and are accurate to $\pm 1\%$ at $H = 0.020$ G.

Table II gives the resonance line signal based on the two-level solution [Eq. (2.5)] and on the three-level solution [Eq. (A16) of the Appendix] for weak fields H. One point of importance obtained from a comparison of these solutions is the effect of state 3 on the line shape for the transition ν_{14}. The line shape from the three-level solution is not Lorentzian and we can estimate from the signal heights at the half-maximum points for the two solutions that an error of about 0.3 ppm would be made at $H = 3$ G by determining the line center with the two-level Lorentzian line shape. This agrees with the estimate of frequency pulling given in Eq. (2.8).

c. *Time-dependent line shape.* The time-dependent resonance line shape for magnetic field $H = 0$ is based on $\langle P_z(t) \rangle$ given by Eq. (2.21). The time-dependent differential signal $dS(\theta, t)$ is

$$dS(\theta, t) = a \cos\theta \, L'(t) K', \quad (2.32)$$

where

$$L'(t) = -\left[1 - \left(\frac{\Gamma_0 + \omega'}{2\Gamma}\right) \cos\left(\frac{\Gamma_0 - \omega'}{2}\right) t \right.$$

$$\left. - \left(\frac{\Gamma_0 - \omega'}{2\Gamma}\right) \cos\left(\frac{\Gamma_0 + \omega'}{2}\right) t \right] \quad (2.32a)$$

and K' is given by Eq. (2.27c). The total time-dependent signal $S(t)$ is obtained with the same assumptions as for Eq. (2.28):

$$S(t) = \mathcal{K}' \int_V \rho a L'(t) \left(\int_D \cos\theta \, d\Omega \right) d\tau , \qquad (2.33)$$

where $\mathcal{K}'$ is given by Eq. (2.28a).

For the weak-field transitions ν_{14} the time-dependent differential signal is based on an equation analogous to Eq. (2.32a) obtained for the two-level case starting from Eq. (2.5) of Muonium III:

$$dS(\theta, t) = a \cos\theta L(t) K , \qquad (2.34)$$

in which

$$L(t) = \frac{4|b|^2}{\Gamma^2} \sin^2\left(\frac{\Gamma t}{2}\right) \qquad (2.34a)$$

and K is given by Eq. (2.5a). A similar expression applied for the weak-field transition ν_{34}.

III. EXPERIMENTAL METHOD AND APPARATUS

A. Introduction

The basic experimental method was very similar to that of the strong-field experiment discussed in detail in Muonium II[2] and Muonium III.[3] Resonance lines have been observed for the weak-field transitions ν_{14} and ν_{34} between the levels (F, M_F) = $(1, \pm 1)$ and $(0, 0)$ at $H \simeq 3$ G, and for the very-weak-field transition $\Delta F = \pm 1$ at $H \simeq 10$ mG. Resonance lines were obtained by varying the applied microwave frequency with fixed magnetic field H and observing the change in the number of decay positrons emitted along the direction of the incoming muon beam. A schematic diagram of the experimental arrangement for the weak-field transition is shown in Fig. 5, and for the very-weak-field transition in Fig. 6.

The measurements reported in this paper took place in four separate runs over a period of about four years, and changes were made in the equipment for the different runs. Our discussion of the apparatus will cover principally its latest version, together with brief comments on earlier versions.

B. Magnetic Field

The low magnetic fields required for the weak- and very-weak-magnetic-field measurements were obtained with the magnetic shield and solenoid system shown in Fig. 7. There were three moly perm-alloy magnetic shells[18] for shielding, and an inner solenoid together with two movable correction coils. Mu-metal end caps[19] could be fastened over the exterior of the outer two shells. The shells were degaussed by passing 15–30 A at 60 Hz through toroidal windings which linked all three shells, and then reducing the current slowly to zero. In the Gibbs Laboratory this degaussing procedure resulted in a field of less than 1 mG inside the shells with the end caps on. During the experiment the field exterior to the shield structure was due primarily to the fringing field of the main cyclotron magnet, and amounted to an approximately vertical field of 5 to 10 G with a field gradient of up to 3 G/m.

For the weak-field measurement at 3 G the end caps were not used and the solenoid and correction coils provided a horizontal field homogeneous to better than 1 part in 10^3 over the region of the microwave cavity (18-cm diameter, 20-cm length).
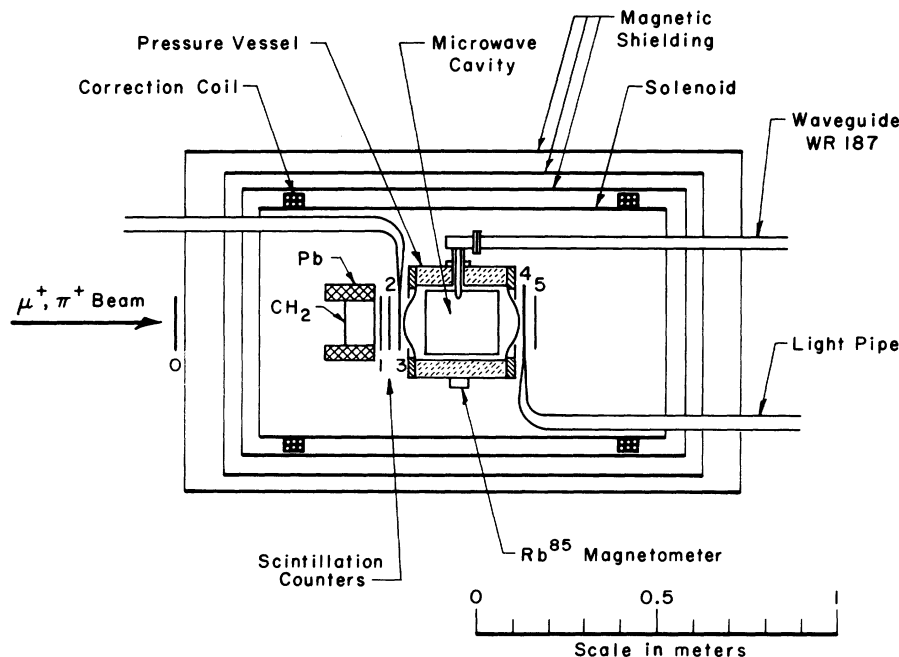

FIG. 5. Schematic diagram of the experimental apparatus used for weak-field transition, showing the target and scintillation counters (numbered 0–5).
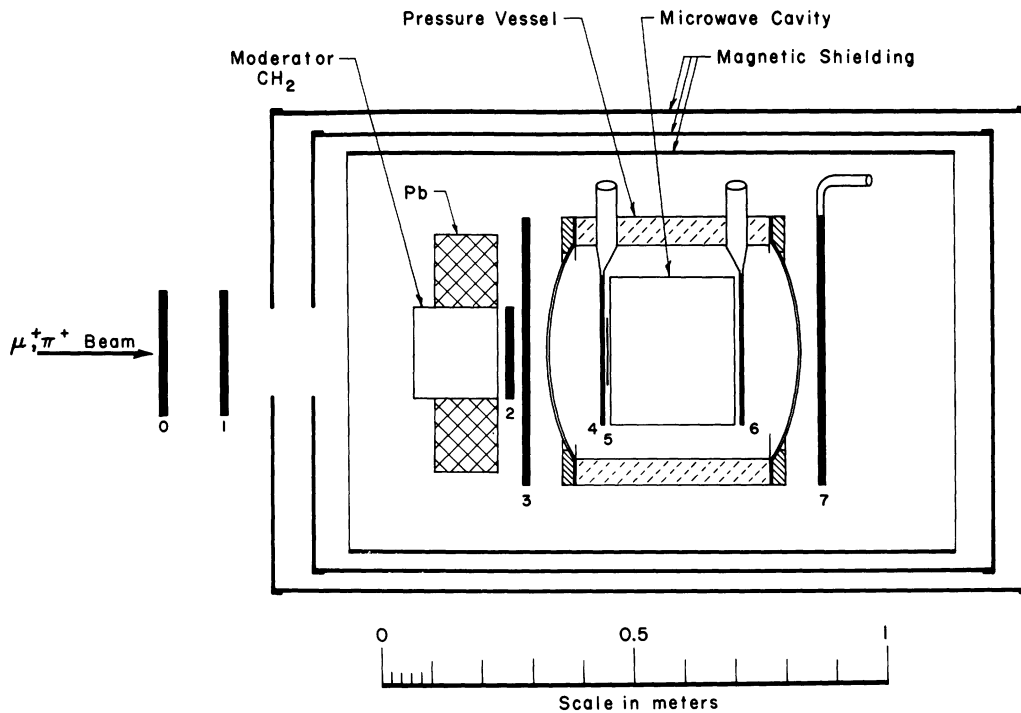
FIG. 6. Schematic diagram of the experimental apparatus used for very weak field transition, showing the target and scintillation counters (numbered 0–7).

The current-regulated power supplies which excited the solenoid and correction coils were regulated to 5 parts in 10^5 and determined the field stability of about 0.5 mG. If the cyclotron magnet or internal solenoid field were changed, the shells were degaussed and then the magnetic field in the region of the microwave cavity could be reproduced to within 1 mG.

For the weak-field measurement at 3 G the magnetic field was mapped and monitored with a rubidium optical-pumping magnetometer of standard design[20] as shown in Fig. 8. An externally heated rubidium rf discharge lamp served as the light source. A field modulation of about 10 mG was applied during the off period for the microwave power and hence at a frequency of 7.5 Hz (see
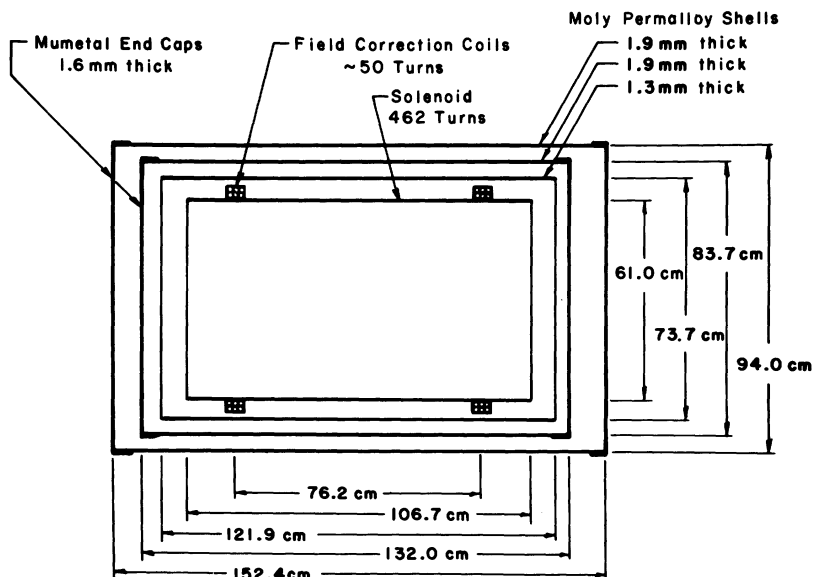

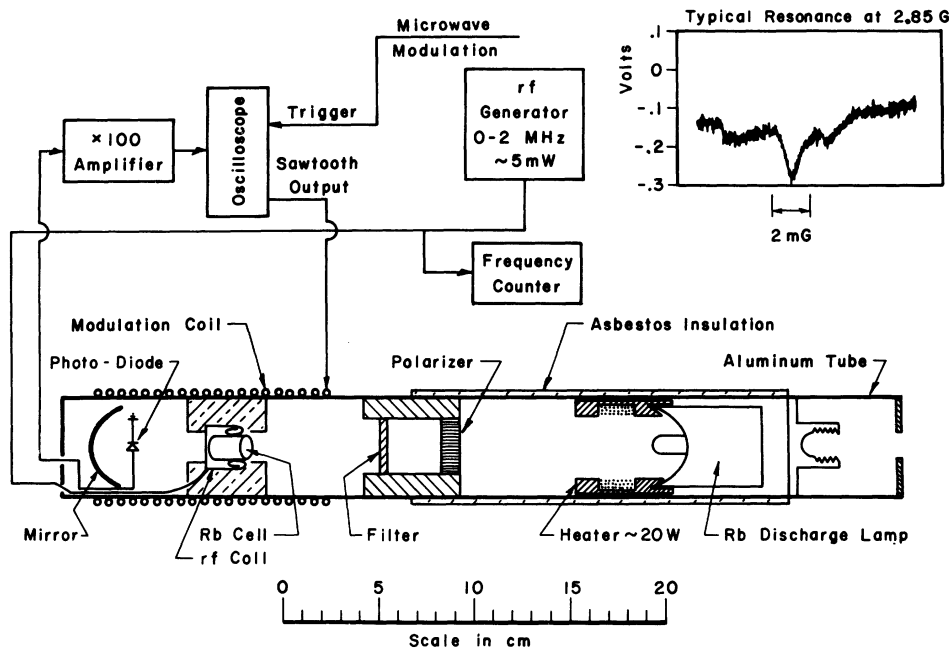FIG. 7. Schematic diagram of the magnetic shield and solenoid system.

FIG. 8. Rubidium optical-pumping magnetometer.

Fig. 12). The optical-pumping resonance signal was detected as a decrease in the light intensity reaching the photodiode. The uncertainty in the magnetic field measurement was due to 60-Hz field modulation associated with ground loop currents and amounted to about 2 mG. The position of the monitor probe during data taking was 18 cm from the axis of the solenoid in its midplane, where the field differed by only 10 mG from that at the center of the microwave cavity.

For the very-weak-field measurement the solenoid was turned off and the Mu-metal end caps were fastened over the two outer moly permalloy shells. The resulting field was from 7 to 13 mG throughout the target volume and had an average value of about 10 mG. Its direction was approximately antiparallel to the incident beam direction. The radial and azimuthal components of H were from 1 to 3 mG.

For the very-weak-field measurement the magnetic field was mapped and monitored with a fluxgate magnetometer.[21] This instrument was convenient to use and also allowed the detection of ac magnetic fields which could be generated by ground loop currents ($\lesssim 0.1$ mG). Using the degaussing procedure for the shells described previously about once a week, or whenever the magnetic field of the cyclotron was changed, the field was maintained constant to within about 0.5 mG.

C. Target and Gas-Handling System

The major features of the target and gas-handling system have been described in the earlier pa-

pers of this series.[1-3] The gas-purifying system was entirely rebuilt and provided a cleaner, more efficient system. High-purity argon and krypton were used.[22] Because of its high cost the krypton was reused for several target fillings by employing a cryogenic pump; the argon was used for only one target filling. For the later measurements[10-12] reported here, a diaphragm pump[23] replaced the magnetically driven piston circulation pump allowing for faster and smoother gas flow and elimination of ground current surges associated with energizing the solenoids of the magnetic pump. The temperature of the target gas was monitored by four copper-constantan thermocouple pairs. The over-all absolute accuracy of each thermocouple pair was ± 0.2 °C, as determined by comparison to a mercury thermometer[24] calibrated by the National Bureau of Standards. The target temperature was stabilized by circulating water through the copper jacket surrounding the pressure vessel. Temperature variations of 2 °C during a 24-h period were typical. The pressure was measured by an autotracking quartz Bourdon tube[25] with an absolute accuracy of about 4 torr or 0.025%, which was determined by calibration against a deadweight gauge.

The data of this paper were obtained with three separate target pressure vessels. The first was shown in Fig. 4 of Muonium III,[3] with the addition of ports for a tuning bar and thermocouples. The second vessel was similar to the first but was 30 cm longer to permit the installation of scintillation counters in the target gas by a scheme similar to
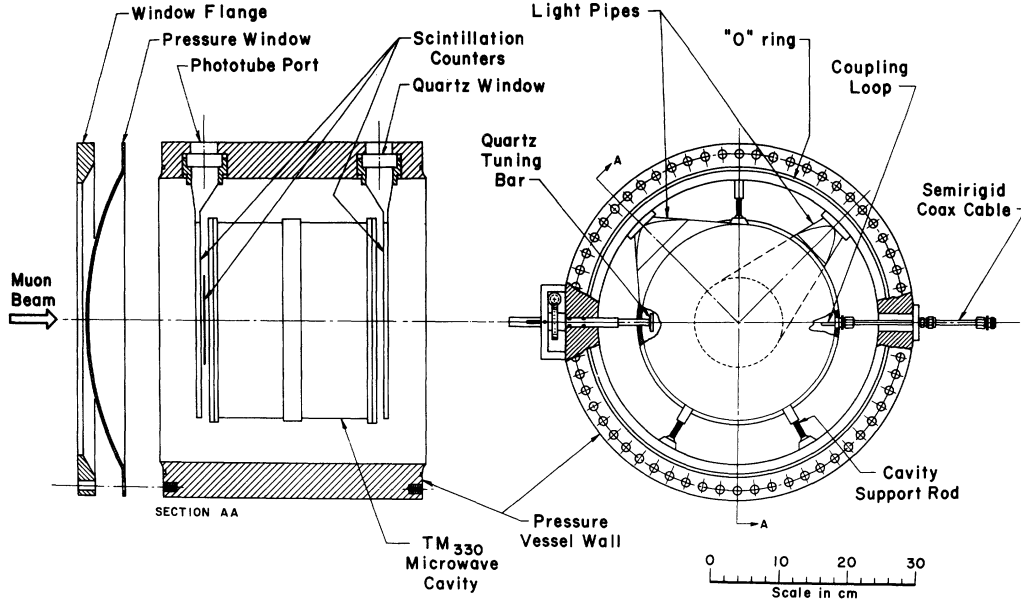
FIG. 9. Pressure vessel and microwave cavity with internal scintillation counters.

that shown in Fig. 9. The most recent pressure vessel incorporated three internal scintillation counters and allowed for a larger-diameter micro-wave cavity (see Fig. 9). The thicknesses of the aluminum end windows of the pressure vessels ranged from 0.05 to 0.5 cm, depending on the pressure used.

D. Cavity and Microwave System

Four different microwave cavities were used, three operating in the TM_{220} mode and one in the TM_{330} mode. The TM mode was chosen to provide a microwave field $\vec{H}_1$ perpendicular to the direction of the incident-muon spins and hence suitable to induce the desired transitions with $\Delta M_F = \pm 1$. It is convenient that the fields in these microwave modes are independent of the axial, or z, position, and that the cavity resonant frequency is independent of the length of the cavity. The cavity diameter required to give a resonant frequency close to $\Delta \nu$ for the TM_{220} mode is about 18 cm, which is a convenient match to the dimension of the muon beam from the Nevis synchrocyclotron. Three different

cavities in the TM_{220} mode were required to accommodate the substantial range in resonant frequency associated with the use of two different gases—argon and krypton—and a wide range of gas pressures. The TM_{330}-mode cavity with a relatively large diameter was used for the final run at our lowest gas pressure of 9.3 atm of Ar in order to minimize the number of muons stopping in the walls of the cavity. Data on the microwave cavities used are given in Table III.

The basic construction of the microwave cavities (see Fig. 9) was similar to that used in Muonium III. They were aluminum cylinders with side-wall thicknesses of about $\frac{1}{4}$ cm and with thin end walls of 0.005 cm thickness. The cavities were supported in the pressure vessel by six adjustable rods between the outer walls of the cavity and the inner wall of the pressure vessel. The small copper input loop of about 1-cm^2 area was attached to a piece of UT250 semirigid microwave coaxial cable on the input connector. Changing the orientation and size of this coupling loop allowed good coupling to be obtained with a voltage–standing-wave ratio of less than 1.1.

For the TM_{220} and TM_{330} modes the squares of the microwave magnetic field intensities are given by[26]

TABLE III. Data on microwave cavities used.

Mode	Diameter (cm)	Length (cm)	Gas	Density range (atm)
TM_{220}	17.808	19.766	Ar	10–30
			Kr	6–20
TM_{220}	17.648	19.603	Ar	40–60
			Kr	30–40
TM_{220}	17.447	19.373	Ar	60–110
			Kr	60
TM_{330}	27.666	24.260	Ar	10–20

$$TM_{lm0}: H_1^2(r,\phi) = \frac{4\pi\mu P Q_{lm}}{\omega_{lm0} V J_{l+1}^2(x_{lm})}$$

$$\times [J_{l+1}^2(x_{lm}r/R) + J_{l-1}^2(x_{lm}r/R)$$

$$- 2J_{l+1}(x_{lm}r/R)J_{l-1}(x_{lm}r/R)\cos(2l\phi)],$$

(3.1)

in which μ is the magnetic permeability of the gas in the cavity; P is the power input to the cavity in watts; Q_{lm} is the unloaded Q of the cavity; ω_{lm0} is the resonant angular frequency of the TM_{lm0} mode; V is the volume of the cavity; J_l is the lth-order Bessel function; $x_{22} = 8.417$ and $x_{33} = 13.015$; R is the radius of cavity.

The required amplitudes of the microwave magnetic field for weak-field and for very-weak-field transitions can be determined approximately from Eqs. (2.6) and (2.27b), respectively, together with the matrix element b given in Table I of Muonium II. For the weak-field transition $(F, M_F) = (1, 1)$ —→ $(0, 0)$ at $H = 3$ G, the muon polarization change (proportional to $|a_1|^2 - |a_4|^2$) will be maximum[3] for $t = 1/\gamma$ if $H_1 = 0.228$ G; for the very-weak-field transitions at $H \simeq 10$ mG, the muon polarization change can be determined to a very good approximation from Eq. (2.21) and is a maximum for $t = 1/\gamma$ if $H_1 = 0.161$ G. With the unloaded Q of 27 000 for the TM_{220} cavity, an input power of about 1 W was required to produce an average H_1 value of 0.16 G over the cavity. For the TM_{330} cavity the unloaded Q was 45 000 and the required input power was also about 1 W. The microwave input power raised the temperature of the cavity by less than 2 °C relative to the wall of the pressure vessel.

FIG. 10. Block diagram of the microwave system.

The TM_{330} cavity was tuned to the driving frequency of the microwave source by means of a movable quartz bar $18 \times 2.5 \times 0.45$ cm. In this experiment the resonance lines were obtained by varying the microwave frequency; a movement of the tuning bar of about 0.08 cm was sufficient to sweep through a resonance line. There was no detectable change in the cavity Q over the frequency range of the resonance line.

The over-all microwave system is shown in Fig. 10. It consisted of the microwave-frequency generating system, the power amplification and stabilization system, and the microwave cavity and its associated tuning mechanism. The microwave-frequency generating system consisted of a frequency synthesizer[27] with 44.6 MHz output, a ×10 frequency multiplier using tuned circuits, a power amplifier,[28] a second stage of ×10 multiplication using a step recovery diode,[29] and a bandpass filter.[30] This system produced an output frequency of about 4463 MHz at a power level of 0.1 mW. The frequency was stable to a few parts in 10^8 by comparison with WWV. The frequency spectrum was symmetric and the spectral width of the signal was less than 1 kHz, as measured with a spectrum analyzer.[31]

Power amplification to an output of several watts was provided by a traveling-wave tube amplifier.[32] The power feedback system with a response time of 1 μsec was used to stabilize the power level to about 1%, as well as to supply a microwave on-off signal for the slow logic and to provide a means for the on-off modulation. The power levels were measured with temperature-stabilized thermistor power meters,[33] which had an absolute accuracy of 3% and a relative accuracy of better than 1%. The changes in reflected power from the cavity were negligible over periods of hours.
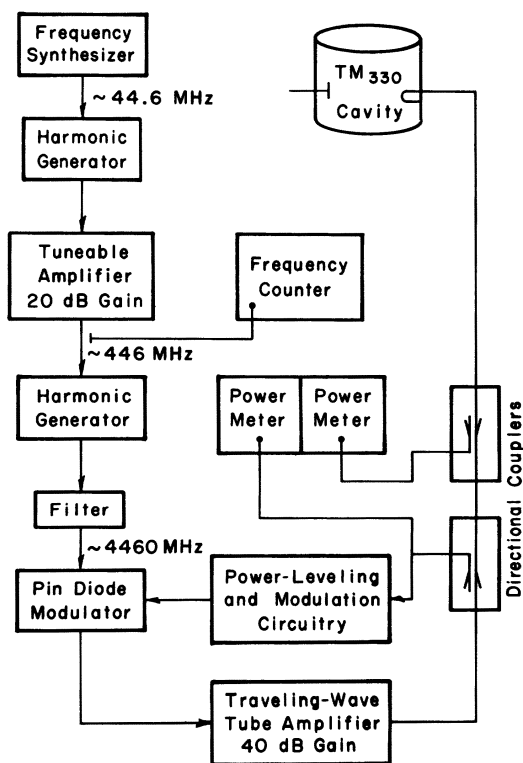
E. Counters and Electronics

The scintillation counter system is indicated in Figs. 5 and 6. The principal differences as compared to the system described in Muonium III are the use of much-larger-area positron counters and the placement of several scintillation counters which define the stopped muons inside of the pressure vessel. The larger-area counters increased significantly the efficiency of positron detection to the value of about 20%. The use of internal counters in the pressure vessel reduced the background counts associated with particles which stop in the pressure windows and in the gas between these windows and the microwave cavity. The inside scintillators were viewed through quartz windows by phototubes[34] fastened directly onto the pressure vessel and had a counting efficiency of greater than
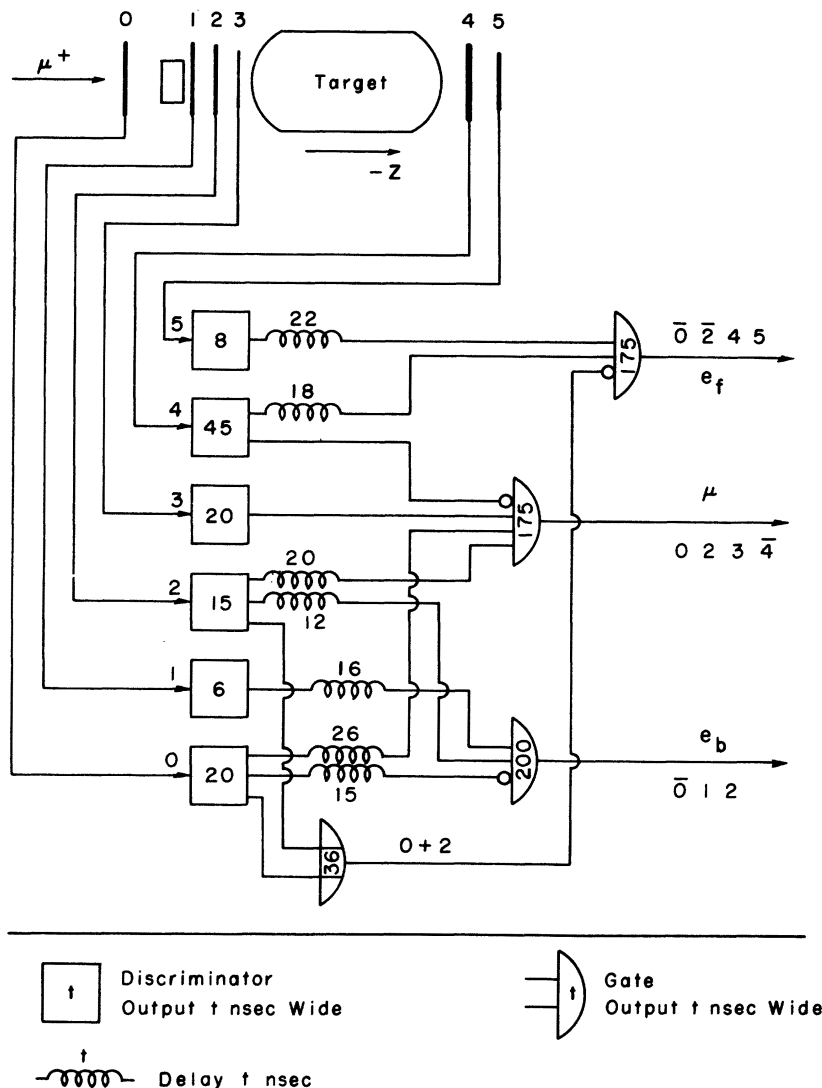
FIG. 11. Block diagram of fast-logic-electronics system. This system was used with the weak-field apparatus shown in Fig. 5; a similar system was used with the very-weak-field apparatus shown in Fig. 6.

96%. These inside scintillators did not contaminate the target gas to the extent that there was any significant reduction in the muonium resonance signal. The so-called forward (backward) resonance signal was obtained with the events E_f (E_b) shown in Figs. 11 and 12.

The fast- and slow-electronic-logic systems used were similar to those described in Muonium III and are shown in Figs. 11 and 12. A PDP-8 computer[35] was used on line in our most recent measurements to monitor and control the experiment in the configuration shown in Fig. 13. Some significant features of this system included (i) use of one set of 24 scalers to collect both the microwave on and off data, (ii) generation of a 10-μsec dead time following a particle stop in the moderator (Fig. 6), (iii) automatic recording with the computer of 20 analog variables such as those mentioned in Sec. III F, and (iv) data recorded on magnetic tape.[36]

A 45-MHz digitron was used to obtain time-dependent signal data (see Fig. 14) by a method similar to that used in Muonium III. The digitron recorded the timing of events in the following manner: For a real (accidental) event the digitron scaler began counting 45-MHz pulses when a μ stop (positron) occurred and ceased counting when a positron (μ stop) occurred. For any other combination of events in a 6-μsec period the scaler and the latches were cleared and the events ignored. If an acceptable real or accidental event occurred, the A and B inputs to the controller were inhibited and a computer interrupt initiated. After the computer read the digitron scaler and latches and stored the results in a buffer, a reset command was given to the digitron controller. Later the computer would process the buffer by incrementing the core word which corresponded to the time and appropriate event type, after verifying that the
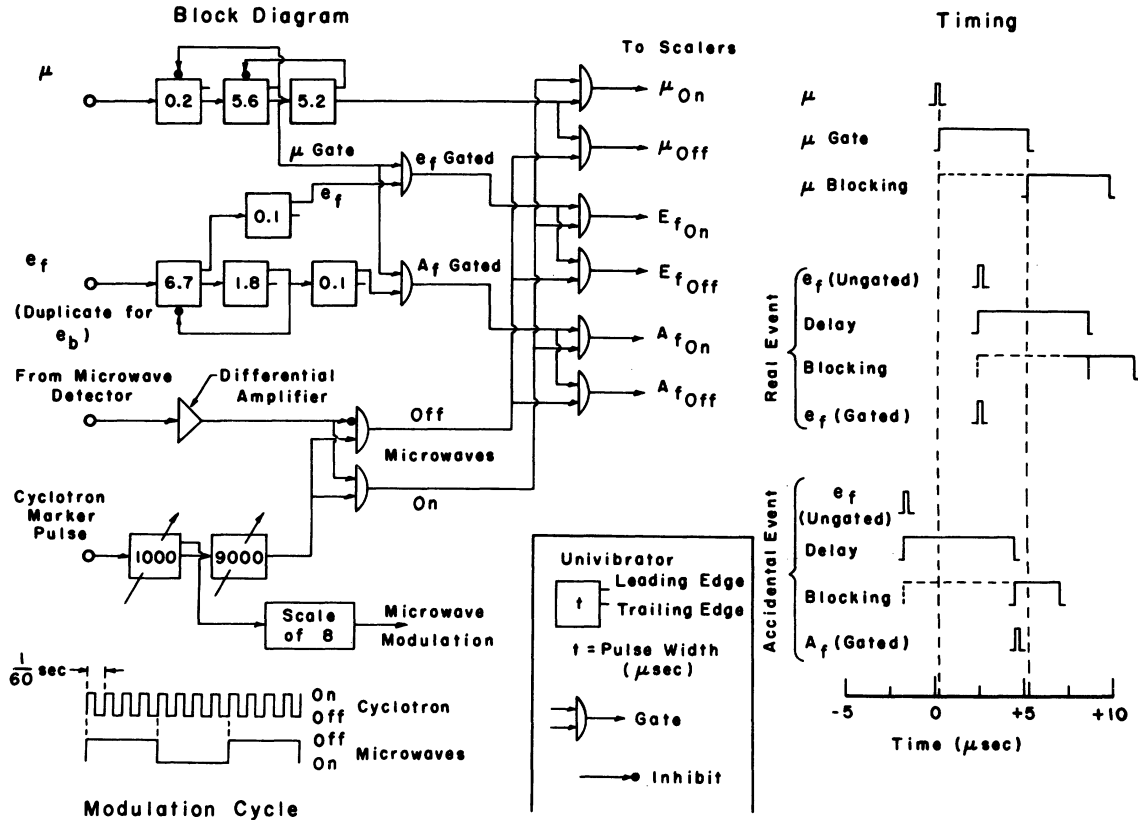
FIG. 12. Block diagram of slow-logic-electronics system. This system was used for all our runs except the latest one; the system for the last run was similar except that a single set of scalers was used to record the microwave on and off data.

event type was valid. The digitron had a maximum counting rate of 75 kHz while the event rate was about 20 Hz, so that dead time was negligible.

F. Procedure of Data Taking

The procedure of data taking was fundamentally the same as for Muonium III. However, one important difference was that the resonance curves were obtained by varying the microwave frequency rather than the magnetic field. For the weak-field transition variation of the microwave frequency was more convenient because of the necessity of having a homogeneous magnetic field over the cavity volume. From Eq. (2.1) for the energy levels and Fig. 2 for the resonance line shapes, it is clear that for the very-weak-field transition no simple resonance line shape would be obtained by varying the magnetic field. As the microwave frequency was varied, the cavity was retuned for each microwave frequency so that the power in the cavity was constant to better than 1% over the resonance linewidth.

The positive-muon beam of the Columbia University Nevis synchrocyclotron was used for our experiment. Its characteristics have been described

in our earlier papers.[1-3] For the present experiment the muon stopping rate was somewhat higher, because of inproved cyclotron operation, and. amounted to about 2000/sec in a target of 6 g/cm^2. The muon beam had a duty factor about 30% with the use of its vibrating target.[37]

Data were taken with the two stopping gases, argon and krypton, over pressure ranges from 10 to 108 atm, and from 6 to 73 atm, respectively. The counter-defined muon stopping rate in the target varied from about 200/sec for 10 atm of argon to about 2000/sec for 108 atm. With 10 atm of argon about $\frac{1}{5}$ of the stopped muons, or 40/sec, stopped in the active gas in the microwave cavity; with 108 atm of argon about $\frac{1}{3}$ of the stopped muons, or 700/sec, stopped in the active-gas region. For the 10-atm-argon case internal counters were used to define the stopping muons, whereas for the 108-atm-argon case only external counters were used. Similar stopping rates were obtained with krypton at the same density as argon.

Typical values of the various scaler rates were similar to those given in Muonium III. In addition to the scaler readings the quantities recorded during data taking included (i) microwave frequen-
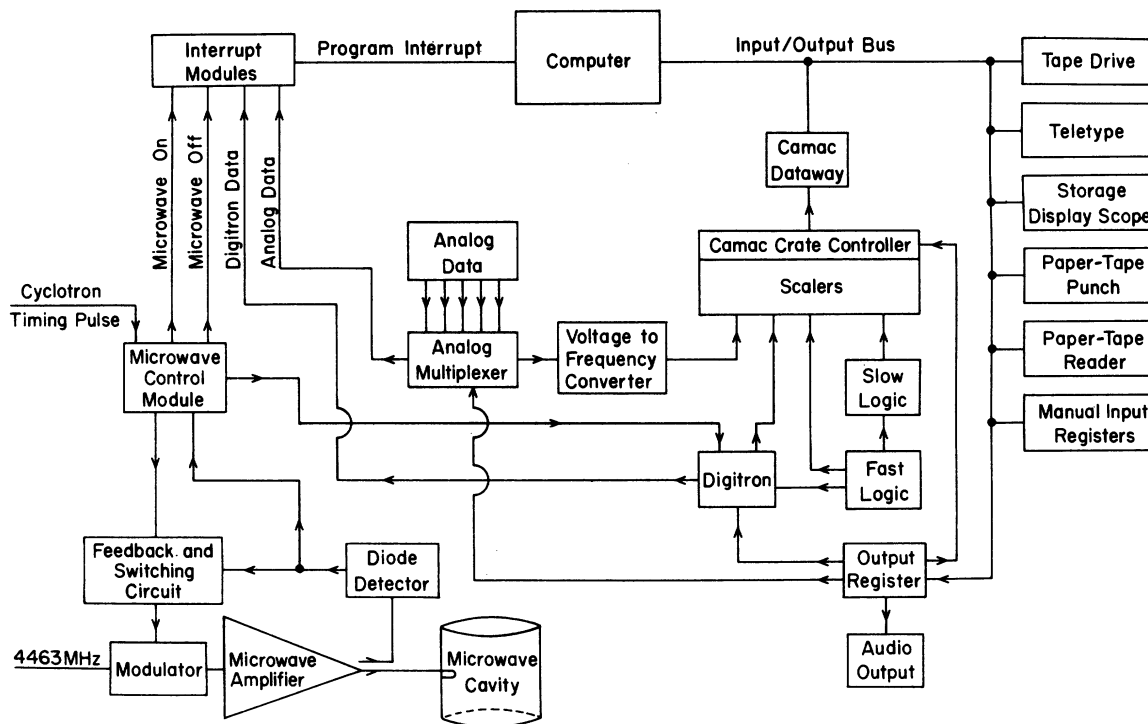
FIG. 13. Schematic diagram of data acquisition system, including the on-line PDP-8 computer.

cy, (ii) static magnetic field, (iii) gas pressure and temperature, (iv) microwave input and output powers for the cavity, (v) getter temperature, and (vi) current in the dipole magnet used to select the momentum of the muon beam. All of the data were accumulated with the PDP-8 computer and written on magnetic tape for later processing; in addition, some of the data were logged manually as a check.

Several time-integrated resonance curves are shown in Fig. 15. Note that for the weak-field case, Fig. 15(a), the linewidth (full width at half-maximum) is about 300 kHz and the signal intensity is 0.45%; both of these values are consistent with the discussion in Sec. II B1. For the resonance lines observed in the very weak field, Figs. 15(b)–15(f), the linewidths are broader, between 500 and 800 kHz, and the signal intensity is between 1.6 and 2.5%. These signal intensities and line-
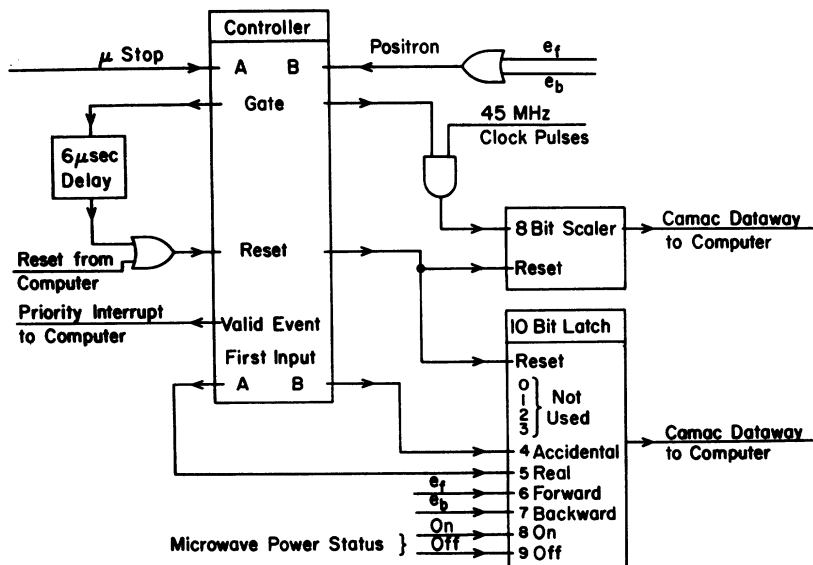

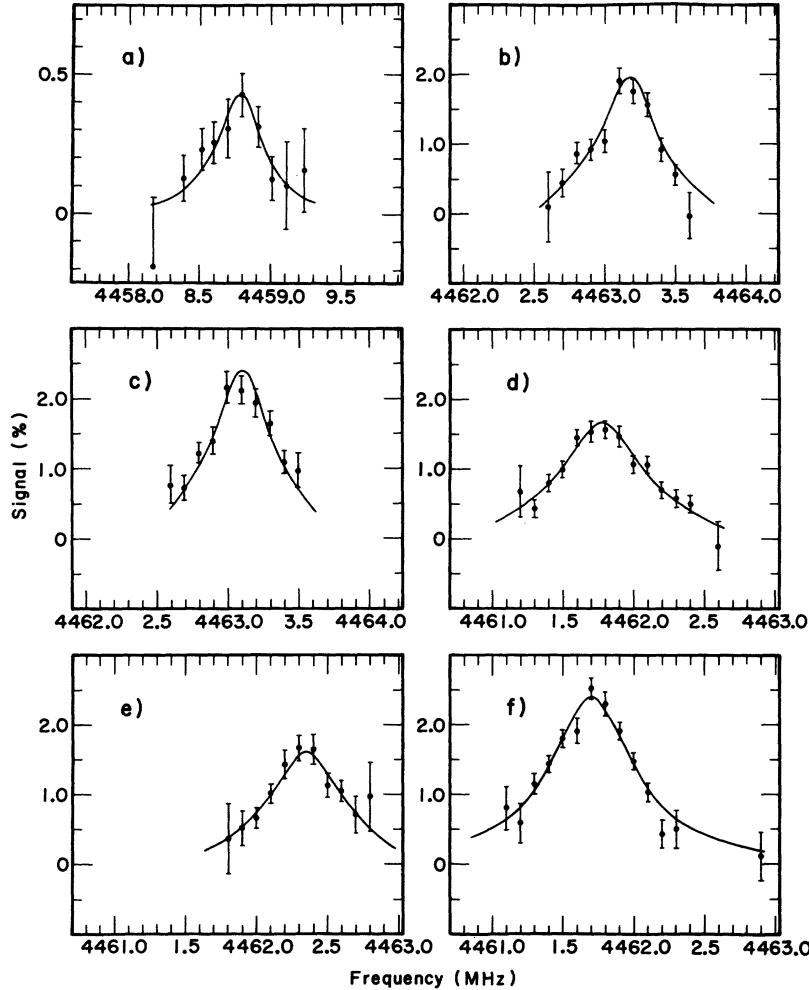FIG. 14. Schematic diagram of 45-MHz digitron system.

FIG. 15. Observed resonance curves obtained with the forward positron telescope. (a) At H = 2.85 G, with 35.1 atm argon; (b) at $H \simeq 10$ mG, with 9.3 atm argon; (c) at $H \simeq 10$ mG, with 13.7 atm argon; (d) at $H \simeq 10$ mG, with 43.2 atm krypton; (e) at $H \simeq 10$ mG, with 64.5 atm argon; (f) at $H \simeq 10$ mG, with 108.7 atm argon.

widths observed at very weak fields are consistent with the discussion in Sec. II B2. A time dependent resonance curve is shown in Fig. 16, which was obtained concurrently with the time integrated resonance curve shown in Fig. 15(b). Lists of the resonance curves obtained with argon and krypton are given in Tables IV and V, respectively.

IV. DATA ANALYSIS

A. Initial Treatment of Data and Determination of Line Centers

The treatment of the data was very similar to that described in Muonium III. Initially the forward and backward signals and their statistical standard deviations are calculated from the formulas[38]

$$y_f = \frac{E_f'/N' - A_f'/N'}{E_f/N - A_f/N} - 1 \qquad (4.1)$$

and

$$\sigma_f = \left[\frac{(E_f' - A_f')/N'}{(E_f - A_f)/N} \right]\left[\frac{E_f(1 - E_f/N) + A_f(1 - A_f/N)}{(E_f - A_f)^2} \right.$$
$$\left. + \frac{E_f'(1 - E_f'/N') + A_f'(1 - A_f'/N')}{(E_f' - A_f')^2} \right]^{1/2},$$

$$(4.2)$$

in which (N, N') is the number of stopped muons, (E_f, E_f') is the number of forward events, and (A_f, A_f') is the number of forward accidental events; the unprimed quantities were obtained with microwaves off and the primed quantities with microwaves on (see Figs. 11 and 12). The corresponding quantities for the backward signals are designated by the subscript b.

These experimental quantities were fitted by a least-squares method to the theoretical line shape given by Eqs. (2.5) and (2.6) for the weak-field case and by Eqs. (2.27), (2.28), and (2.31) for the very-weak-field case. The parameters in the fit were the line-center frequency ν_0, the height of the signal at
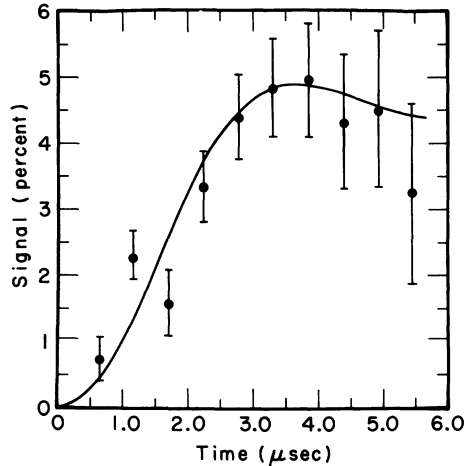
FIG. 16. Observed signal height as a function of time for the very-weak-field transition with $H \simeq 10$ mG, with argon at 9.3 atm, with microwave frequency $\nu = 4463.200$ MHz, and with input microwave power of 1 W. The 1-standard-deviation error bars are due to counting statistics. The solid curve is a fit of Eq. (2.33) to the time-dependent data with resonance frequency $\nu_0 = 4463.162 \pm 0.010$ MHz.

resonance, and the linewidth. Values for ν_0 and the signal height were determined for a series of values of linewidth consistent within a factor of 2 with the measured microwave input power and cavity Q. The value of ν_0 varied by less than $\frac{1}{2}$ standard deviation over the range of linewidths chosen. Typical fitted resonance lines are shown in Fig. 15. The results of the analysis of all the resonance lines are given in Tables IV and V for argon and krypton, respectively. The errors in the line centers are 1-standard-deviation errors due to statistical counting.

Additional analyses of some of the lines observed at very weak field were done using the line-shape theory for $H = 0$ given in Eq. (2.28), in which a uniform muon stopping distribution over the microwave cavity was assumed. Also an approximate solution for the very-weak-field case given in Eq. (2.31) was used, the measured values of magnetic field were employed, and a uniform muon stopping distribution was again assumed. For the weak-field case additional analyses were made based on Eq. (2.5), which took into account the measured values of the magnetic field, the variation of microwave power over the cavity, and the detector solid angles, and assumed a uniform muon stopping distribution. The results of these analyses were within $\frac{1}{4}$ standard deviation of the results based on the simpler method discussed in the preceding paragraphs.

The time-dependent data obtained with the digitron were fitted by a line shape based on Eq. (2.32);

the variation in microwave power over the cavity was included and a uniform muon stopping distribution was assumed. The parameters in the fit were the resonance frequency ω_0, a signal amplitude, and the microwave power. A typical fitted time-dependent resonance line is shown in Fig. 16. Because of the additional information contained in the time-dependent data, a higher accuracy is achieved in the determination of ω_0 than from the data for time-integrated resonance curves such as shown in Fig. 15. The improvement in statistical accuracy is about 40% with the time-dependent data. The results of the analysis with the time-dependent data agreed well with the results based on the time-integrated resonance curves in Fig. 15. In principle, fitting the time-dependent data makes possible the determination of the microwave power in the cavity at each frequency. There was no observed variation of microwave power with frequency within the 5% accuracy of the determination. For the present data this method is less precise than the direct power measurements which were made to about 2%.

B. Extrapolation to Zero Gas Density

The experimental data of Tables IV and V were fitted to the function

$$\Delta\nu(D) = \Delta\nu(1 + aD + bD^2) , \qquad (4.3)$$

in which D is the gas density, a is the coefficient of the linear density shift, and b is the coefficient of the quadratic density shift. Measurements at slightly different densities were grouped after correcting for the dependence of $\Delta\nu$ on D. The grouped data were then fitted to Eq. (4.3). This procedure increased the sensitivity of the fit to the parameters a and b. Figure 17 shows a plot of the grouped values of $\Delta\nu$ as a function of the target-gas density for argon and krypton. The results of least-squares fit are shown in Table VI for the two cases: (i) a is a free parameter, $b \equiv 0$, and (ii) both a and b are free parameters. These results indicate clearly that adequate fits for argon require a nonzero value for the quadratic coefficient b, and for krypton a nonzero value for b is favored. Furthermore the fits with the quadratic term yield satisfactory agreement between the values for $\Delta\nu$ from the argon and krypton data, as is necessary. Figures 18 and 19 compare the fits with and without the quadratic term for argon and krypton, respectively. Hence we choose the fits with the quadratic term and the results for $\Delta\nu$ based on the argon and krypton data are

$$\Delta\nu = 4463.312 \pm 0.013 \text{ MHz}, \text{ with argon} \qquad (4.4a)$$

$$\Delta\nu = 4463.293 \pm 0.023 \text{ MHz}, \text{ with krypton.} \qquad (4.4b)$$

TABLE IV. Results of analysis of resonance curves with argon.

Gas density[a] (torr at 0 °C)	Temperature (°C)	Number of muons stopped (10^8)	Signal size[b] (%)	Linewidth[c] (kHz)	Line center[d] (kHz)
7100	21.5	2.0	2.9	520	$4\,463\,162 \pm 10$[e,f]
10392	23.5	1.7	3.7	590	$4\,463\,089 \pm 11$[e,f]
24306	24	2.5	3.3	800	$4\,462\,754 \pm 32$[g]
24487	17	5.1	2.3	1140	$4\,462\,783 \pm 30$[g]
24487	16	4.8	2.5	1130	$4\,462\,752 \pm 32$[g]
24528	17	4.6	2.3	1150	$4\,462\,803 \pm 30$[g]
24720	16	5.0	2.2	1170	$4\,462\,786 \pm 38$[g]
26685[h]	24	14.6	0.8	300	$4\,462\,746 \pm 31$[g]
46104	20	2.9	3.2	1020	$4\,462\,348 \pm 33$[g]
49051	21	4.3	4.1	1140	$4\,462\,341 \pm 22$[g]
82640	19	0.8	4.5	1100	$4\,461\,718 \pm 12$[e,i]

[a]The measured pressure and temperature have been corrected for the real gas pressure-volume relationship to give density in units of 1 atm at 0°C, and the result multiplied by 760 to give density in torr.

[b]The signal size given is the sum of the absolute values of the forward and backward signal heights.

[c]The linewidth is the full width at half-maximum.

[d]The line center given is the result of a least-squares fit, and the associated error is 1 standard deviation, due only to counting statistics.

[e]T. Crane, D. Casperson, P. Crane, P. Egan, V. W. Hughes, R. Stambaugh, P. A. Thompson, and G. zu Putlitz, Phys. Rev. Letters **27**, 474 (1971); P. A. Thompson, D. Casperson, P. Crane, T. Crane, P. Egan, V. W. Hughes, G. zu Putlitz, and R. Stambaugh, in *Proceedings of the International Conference on Precision Measurements and Fundamental Constants*, edited by D. N. Langenberg and B. N. Taylor, Natl. Bur. Stds. Publ. No. 343 (U. S. GPO, Washington, D. C., 1971), p. 339.

[f]Result of fit to time-dependent data. The time-integrated signal was also recorded and fitted and is in agreement with this value. The data were taken with internal counters.

[g]P. A. Thompson, J. J. Amato, P. Crane, V. W. Hughes, R. M. Mobley, G. zu Putlitz, and J. E. Rothberg, Phys. Rev. Letters **22**, 163 (1969).

[h]This entry is the result of combining seven individual resonance lines for the weak-field transitions ν_{14} and ν_{34} at $H=2.731$ G and $H=2.853$ G and with microwave input powers of 1.5 and 7.0 W, obtained with gas densities in the neighborhood of the indicated value. In determining the value of $\Delta\nu$, Eq. (2.3) was used to extrapolate to zero magnetic field, and normalization to a single gas density was done taking into account the dependence of $\Delta\nu$ on density (see Sec. IV B).

[i]P. Crane, J. J. Amato, V. W. Hughes, D. M. Lazarus, G. zu Putlitz, and P. A. Thompson, in *High Energy Physics and Nuclear Structure*, edited by S. Devons (Plenum, New York, 1970), p. 677.

The final experimental value for $\Delta\nu$ can be chosen as the weighted average value of Eqs. (4.4a) and (4.4b) to yield

$$\Delta\nu = 4463.308 \pm 0.011 \text{ MHz} \quad (2.5 \text{ ppm}), \quad (4.5)$$

where the error is the 1-standard-deviation statistical counting error.

C. Systematic Errors

The systematic errors considered are all small compared to the statistical counting errors. A list of possible sources of systematic errors and estimates of the upper limits of their contributions follows.

(i) Uncertainty in the relative microwave power level in the cavity as the frequency was varied through the resonance line was significant. A linear variation of power with frequency amounting to 2% over the linewidth would produce an asymmetric line shape and could lead to an error in $\Delta\nu$ of 5 kHz or 1 ppm.

(ii) Uncertainty in the microwave frequency was

0.1 kHz and corresponded to an error in $\Delta\nu$ of 0.1 kHz or 0.03 ppm.

(iii) For the weak-magnetic-field case the inhomogeneity of the 3-G field amounted to less than 3 mG and the field instability was about 0.5 mG. The corresponding error in $\Delta\nu$ from a single resonance line could be as large as 2 kHz or 0.5 ppm. For the very-weak-magnetic-field case the inhomogeneity of the 10-mG field amounted to ± 3 mG and the corresponding error in $\Delta\nu$ is negligible. The field instability at very weak magnetic field was about 0.5 mG, and the corresponding error in $\Delta\nu$ from a single resonance line is 0.5 kHz or 0.1 ppm. For many resonance lines the error due to field instability would be reduced.

(iv) The discussion in Sec. II B assumed that the direction of the incident muon beam was along the negative z direction and that the microwave field $\vec{H}_1$ is perpendicular to $\vec{H} = H\vec{k}$. If the direction of the incident muon beam is not exactly along the negative z direction, the initial z component of the muon polarization is slightly decreased. If $\vec{H}_1$ has

TABLE V. Results of analysis of resonance curves obtained with krypton.

Gas density[a] (torr at 0 °C)	Temperature (°C)	Number of muons stopped (10^8)	Signal size[b] (%)	Linewidth[c] (kHz)	Line center[d] (kHz)
4328	26	5.0	2.0	600	$4\,463\,066 \pm 30$[e,f]
7292	18	1.0	1.1[g]	605	$4\,462\,906 \pm 40$[e,f]
7328	10	2.1	4.1	710	$4\,462\,975 \pm 34$[e,f]
7349	15	2.5	3.5	850	$4\,462\,998 \pm 59$[e,f]
7581	16	2.5	2.6	850	$4\,462\,921 \pm 33$[e,f]
15876	21	3.3	2.9	1280	$4\,462\,578 \pm 38$[h]
15928	21	3.8	2.8	840	$4\,462\,578 \pm 25$[h]
15928	19	2.4	2.0	1140	$4\,462\,558 \pm 36$[h]
15959	19	3.7	2.3	770	$4\,462\,554 \pm 26$[h]
16057	19	5.3	2.2	800	$4\,462\,558 \pm 23$[h]
32854	21	5.8	3.2	810	$4\,461\,782 \pm 16$[h]
33951	14	1.7	4.4	1120	$4\,461\,719 \pm 21$[e]
55200	19	1.4	3.9	805	$4\,460\,809 \pm 11$[e]

[a]The measured pressure and temperature have been corrected for the real gas pressure-volume relationship to give density in units of 1 atm at 0 °C, and the result multiplied by 760 to give density in torr.

[b]The signal size given is the sum of the absolute values of the forward and backward signal heights.

[c]The linewidth is the full width at half-maximum.

[d]The line center given is the result of a least-squares fit and the associated error is 1 standard deviation, due only to counting statistics.

[e]P. Crane, J. J. Amato, V. W Hughes, D. M. Lazarus, G. zu Putlitz, and P. A. Thompson, in *High Energy Physics and Nuclear Structure*, edited by S. Devons (Plenum, New York, 1970), p. 677; T. Crane, D. Casperson, P. Crane P. Egan, V. W. Hughes, R. Stambaugh, P A. Thompson, and G. zu Putlitz, Phys. Rev. Letters **27**, 474 (1971).

[f]The data were taken with internal counters.

[g]No backward signal was obtained for this resonance line.

[h]P. A. Thompson, J. J. Amato, P. Crane, V. W. Hughes, R. Mobley, G. zu Putlitz, and J. E. Rothberg, Phys. Rev. Letters **22**, 163 (1969).

a small component in the z direction, the $\Delta M_F = 0$ transition ν_{24} can be induced, but there will be no appreciable shift in the line center.

(v) Uncertainty in the target-gas density associated with a temperature measurement to ± 0.5 °C and a pressure measurement to ± 4 torr amounted to about 0.2%. The corresponding error in $\Delta\nu$ was 1 kHz or 0.2 ppm.

(vi) For the data shown in Tables IV and V the temperature ranged from 10 to 26 °C, but most of the data were obtained from 16 to 24 °C. Because of the dependence of the linear coefficient a in Eq. (4.3) on temperature,[39,40] an error is made in determining $\Delta\nu$ by fitting the data $\Delta\nu(D)$ to Eq. (4.3). Correction of the data in Table IV for argon using the measured value for the temperature dependence for a for hydrogen in argon yields a change in $\Delta\nu$ of less than 0.01 kHz or 0.002 ppm, even though some individual data points changed by as much as 4 kHz. No data on the temperature dependence for krypton are available and hence no attempt has been made to estimate a correction for the krypton data.

(vii) Different approximations in the derivation of the theoretical line shape lead to slightly different line shapes for fitting the data as discussed in Secs. II and IV A. A maximum difference of 3 kHz

in the determination of the center of a single resonance line was obtained with the different approximations and corresponds to an error in $\Delta\nu$ of 0.7 ppm.

Our final experimental value for $\Delta\nu$ is taken to be

$$\Delta\nu = 4463.308 \pm 0.011 \text{ MHz} \quad (2.5 \text{ ppm}). \quad (4.6)$$

The value for $\Delta\nu$ is that given in Eq. (4.5); the 1-standard-deviation error is obtained by adding in quadrature the counting error in Eq. (4.5) and $\frac{1}{2}$ of each of the upper limits of systematic error given above. The systematic-error estimations did not contribute significantly to the final error.

V. RESULTS AND DISCUSSION

The final result of our measurement of $\Delta\nu$ from weak-field and very-weak-field transitions is given in Eq. (4.6) as

$$\Delta\nu = 4463.308(11) \text{ MHz} \quad (2.5 \text{ ppm}). \quad (5.1)$$

This result agrees with our earlier measurement of $\Delta\nu$ from a strong-field transition[3,41]:

$$\Delta\nu = 4463.24(12) \text{ MHz} \quad (27 \text{ ppm}). \quad (5.2)$$

The result of Eq. (5.1) also agrees with the Chicago result from a strong-field transition,[42]
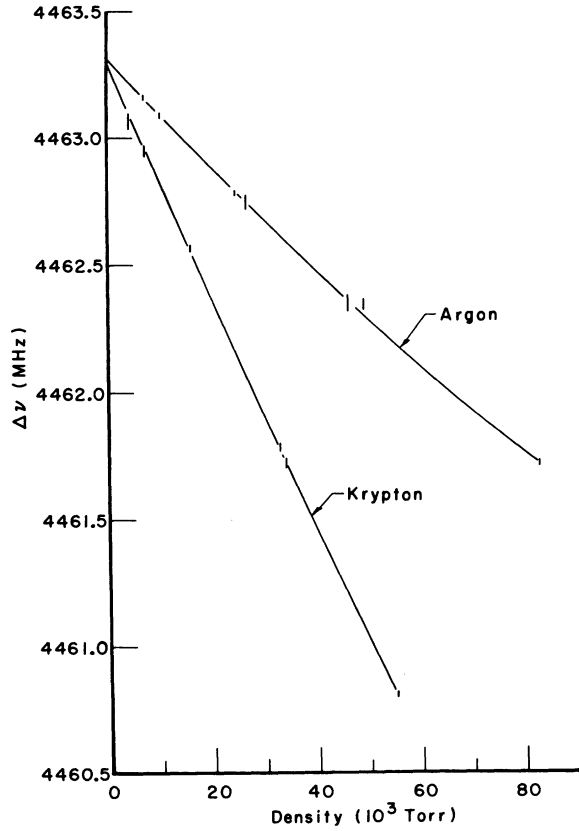
FIG. 17. Experimental values for $\Delta \nu$ vs gas density for argon and krypton. The solid curves are the least-squares fits to the data, including both the linear and quadratic density terms in Eq. (4.3). The error bars represent 1 standard deviation.
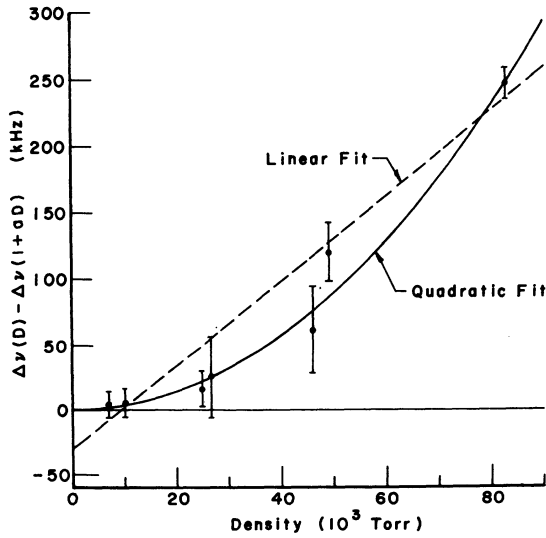
TABLE VI. Results of fits of the data $\Delta \nu(D)$ on the muonium hfs interval at different gas densities to the expression $\Delta \nu(D) = \Delta \nu(1 + aD + bD^2)$.

Gas	a $(10^{-9}/\text{torr})$	b $(10^{-15}/\text{torr}^2)$	$\chi^2/\text{degrees}$ of freedom	$\Delta \nu$ (kHz)
Ar (a free, $b \equiv 0$)	$-4.27(4)$	0	13.3/5	4 463 281(8)
Ar (a, b free)	$-5.00(22)$	8.1(2.5)	3.4/4	4 463 312(13)
Kr (a free, $b \equiv 0$)	$-10.01(7)$	0	4.8/4	4 463 266(13)
Kr (a, b free)	$-10.57(39)$	8.6(5.9)	2.7/3	4 463 293(23)

$$\Delta \nu = 4463.3022(89) \text{ MHz} \quad (2.0 \text{ ppm}) , \qquad (5.3)$$

and with the most precise value yet quoted from the Chicago group based on a very-weak-field experiment by the separated-oscillating-fields method,[7]

$$\Delta \nu = 4463.3012(23) \text{ MHz} \quad (0.5 \text{ ppm}) . \qquad (5.4)$$

The most recent theoretical formula for $\Delta \nu$ was given in Muonium III[3,43]:

$$\Delta \nu_{\text{theor}} = [\tfrac{16}{3} \alpha^2 c R_\infty (\mu_\mu / \mu_B^e)] [1 + (m_e / m_\mu)]^{-3}$$
$$\times (1 + \tfrac{3}{2} \alpha^2 + a_e + \epsilon_1 + \epsilon_2 + \epsilon_3 - \delta_\mu') , \qquad (5.5)$$

where

$$a_e = \alpha / 2\pi - 0.328\,48\,\alpha^2/\pi^2$$
$$+ (1.29 \pm 0.06)\alpha^3/\pi^3 \qquad (\text{Ref. 44}) ,$$

$$\epsilon_1 = \alpha^2 (\ln 2 - \tfrac{5}{2}) , \quad \epsilon_2 = -(8\alpha^3/3\pi) \ln\alpha (\ln\alpha - \ln 4 + \tfrac{281}{480}) ,$$

$$\epsilon_3 = (\alpha^3/\pi)(18.4 \pm 5) ,$$

$$\delta_\mu' = (m_e / m_\mu)\{(3\alpha/\pi) [1 - (m_e/m_\mu)^2]^{-1} \ln(m_\mu/m_e)$$
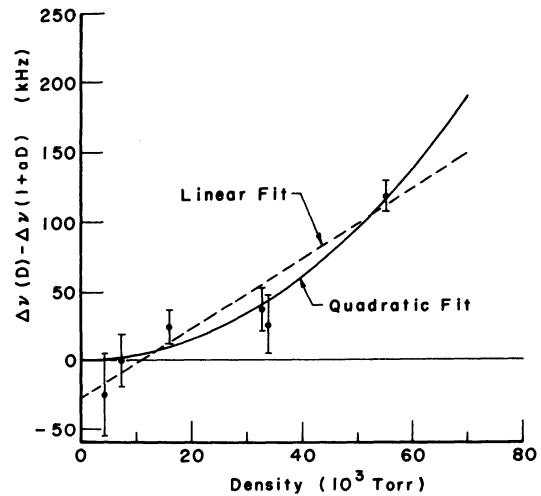$$+ \tfrac{9}{2} \alpha^2 \ln\alpha [1 + (m_e/m_\mu)]^{-2}\} ,$$

FIG. 18. Comparison of linear and quadratic fits to data $\Delta \nu(D)$ for argon. The data are presented in the functional form $[\Delta \nu(D) - \Delta \nu(1 + aD)]$, in which $\Delta \nu = 4463.312$ (13) MHz and $a = -5.00(22) \times 10^{-9}/\text{torr}$ were taken from the quadratic fit for argon (Table VI).

FIG. 19. Comparison of linear and quadratic fits to data $\Delta \nu(D)$ for krypton. The data are presented in the functional form $[\Delta \nu(D) - \Delta \nu(1 + aD)]$, in which $\Delta \nu = 4463.293(23)$ MHz and $a = -10.57(39) \times 10^{-9}/\text{torr}$ were taken from the quadratic fit for krypton (Table VI).

in which α is the fine-structure constant, c is the velocity of light, R_∞ is the Rydberg constant, μ_μ is the muon magnetic moment, μ_B^e is the electron Bohr magneton $(e\hbar/2m_e c)$, m_e is the electron mass, and m_μ is the muon mass.

We use essentially the same values of the fundamental constants as for Muonium III:

$c = 2.997\,924\,562(11) \times 10^{10}$ cm/sec (0.004 ppm)

$\hfill$ (Ref. 45),

$R_\infty = 1.097\,373\,12(11) \times 10^5$ cm^{-1} (0.1 ppm)

$\hfill$ (Ref. 46),

$\mu_p/\mu_e = 0.001\,519\,270\,83(46)$ (0.3 ppm) (Ref. 46),

$\alpha^{-1} = 137.036\,02(21)$ (1.5 ppm) (Ref. 46),

$\mu_\mu/\mu_p = 3.183\,346\,7(82)$ (2.6 ppm) (Ref. 47),

$m_\mu/m_e = 206.7682(5)$ (2.6 ppm).

This value of m_μ/m_e is based on the formula

$$m_\mu/m_e = (\mu_p/\mu_\mu)(\mu_e/\mu_p)|g_\mu/g_e|,$$

and the latest experimental values are used for g_μ and g_e,

$g_\mu = -2[1.001\,166\,16(31)]$ (0.3 ppm) (Ref. 48),

$g_e = 2[1.001\,159\,656\,7(35)]$ (0.004 ppm) (Ref. 49).

Note that the velocity of light c has recently been determined with a much increased precision. Hence we obtain

$$\Delta\nu_{\text{theor}} = \alpha^2(\mu_\mu/\mu_p)(2.632\,958\,4 \times 10^7 \pm 1 \text{ ppm}),$$

$\hfill$ (5.6)

$$\Delta\nu_{\text{theor}} = 4463.325 \pm 0.018 \text{ MHz} \quad (4.1 \text{ ppm}).$$

$\hfill$ (5.7)

The major part of the uncertainty in Eq. (5.6), specifically 0.6 ppm, is associated with the inaccuracy of the calculation of the ϵ_3 term[50]; the remainder comes from the uncertainty in the constants R_∞ and μ_p/μ_e. No attempt is made to estimate the uncertainty due to still-higher-order terms, including the $\alpha^2(m_e/m_\mu)$ term in δ_μ', which have not yet been calculated. The uncertainty in Eq. (5.7) is due about equally to the uncertainties in the values of α and of μ_μ/μ_p.

Our experimental value in Eq. (5.1) is in good agreement with the theoretical value of Eq. (5.7). This agreement provides a sensitive, important test of the validity of muon electrodynamics, including the assumption that the muon is a "heavy electron."[51,52]

Indeed, in view of the quoted uncertainty of 2.8 ppm in the value of μ_μ/μ_p and of the subtle physical-chemistry arguments required in its deduction

from the basic experimental observation of the muon precession frequency and proton NMR frequency in liquids, it is probably most useful at present to assume the validity of Eq. (5.5) and to use our measured value of $\Delta\nu$ together with Eq. (5.6) and the measured value of α to determine a value for μ_μ/μ_p:

$$\mu_\mu/\mu_p = 3.183\,335(13) \quad (4.0 \text{ ppm}), \quad (5.8)$$

where the error is determined about equally by the uncertainty in our value of $\Delta\nu$ and in the value of α. This result can then be used to determine the ratio of muon mass to electron mass:

$$\frac{m_\mu}{m_e} = \left(\frac{\mu_p}{\mu_\mu}\right)\left(\frac{\mu_e}{\mu_p}\right)\left|\frac{g_\mu}{g_e}\right| = 206.768\,93(82) \quad (4.0 \text{ ppm}),$$

$\hfill$ (5.9)

in which we have used the experimental value[48,49]

$$|g_\mu/g_e| = 1.000\,006\,50(30) \quad (0.3 \text{ ppm}).$$

The present experiment has determined the linear and quadratic coefficients of the hfs density shift for muonium in argon and krypton. The results (Table VI) are based entirely on our experimental data given in this paper:

$$a_{M\text{-Ar}} = -5.00(22) \times 10^{-9}/\text{torr},$$

$$b_{M\text{-Ar}} = 8.1(2.5) \times 10^{-15}/(\text{torr})^2,$$

$$a_{M\text{-Kr}} = -10.57(39) \times 10^{-9}/\text{torr},$$

$\hfill$ (5.10)

$$b_{M\text{-Kr}} = 8.6(5.9) \times 10^{-15}/(\text{torr})^2.$$

These values were obtained at a temperature of approximately 20 °C. Our results agree well with results reported by the Chicago group,[8] which are based on our data as well as theirs.

In Muonium III it was pointed out that no quantitative theory has yet been given for the values of the linear coefficients a of the hfs density shift for muonium in argon and krypton. Recently, theoretical estimates of the values of the quadratic coefficients b for muonium in argon and krypton have been given.[53] Precise measurements have been made of the a values for the hydrogen isotopes hydrogen, deuterium, and tritium in argon[39] and of a for hydrogen in krypton,[54] but there are no results on the b coefficients for hydrogen. Our results for the a coefficients given in Eq. (5.10) are in agreement with the experimental values for hydrogen, and hence indicate that no difference between a for muonium or the other hydrogen isotopes has been observed within the experimental accuracies. A dependence of the a value on the hydrogen isotope involved is predicted theoretically[55]; however, no quantitative calculations of the isotope dependence have been made for collisions with argon or krypton.

The principal source of error in our experimental determination of $\Delta\nu$ given in Eq. (5.1) is associated with the limited muon-beam intensity available. The low beam intensity resulted in a large statistical counting error and also in the use of relatively high pressure for the stopping gas, and hence in a relatively large hfs pressure shift together with its associated uncertainty. Soon muon beams with intensities of 10^2 to 10^4 times greater will be available at the new meson factories or factorettes (LAMPF, SIN, TRIUMF, NEVIS).[56] With these high-intensity beams it will be possible to reduce the statistical counting errors to a relatively negligible contribution to the total error, which will then be determined by systematic errors. Various approaches are now available for studying the resonance lines, including the conventional single-oscillatory-field method used in this paper, and the important separated-oscillating-fields method applied by Telegdi *et al.* to their study of very-weak-field transitions.[7] A third method related to the time-dependent resonance involves observing the resonance with a single oscillatory field, but only for "old" muonium which has been subjected to a relatively weak microwave field for a time longer than the muon mean lifetime; this method, like the method of separated oscillating fields, achieves a linewidth narrower than the natural width but at the cost of a loss of intensity. It seems clear that in future experiments an accuracy of 0.1 ppm or better will be obtained in the determination of $\Delta\nu$, and of 1 ppm or better in the determination of μ_μ/μ_p.

ACKNOWLEDGMENTS

APPENDIX: LINE SHAPE FOR A LOW MAGNETIC FIELD

The resonance line shape for a low magnetic field in the direction of the incident muon polarization can be obtained by the following steps. (i) The differential equations for the state amplitudes [Eq. (2.9)] are decoupled. (ii) The general form of the time dependence of the state amplitudes is obtained from the decoupled differential equations. (iii) The constants appearing in the general solutions for the state amplitudes are evaluated. (iv) The time dependence of the muon polarization is obtained from the state amplitudes. (v) The resonance line shape is then obtained from the time integral of the muon polarization.

In performing the above steps two approaches were utilized. In the first approach a computer was used to evaluate the constants appearing in the general equations for the state amplitudes, and then the computer completed the remaining steps to obtain the resonance line shape. Figure 2 was obtained with this approach. In the second approach, which will be outlined in this appendix, an analytic expression is obtained for the line shape. Tables I and II and Figs. 3 and 4 were obtained with this second approach.

The derivation of the line shape begins with the coupled differential equations for the state amplitudes [Eq. (2.9)]:

$$
\begin{pmatrix} \dot{a}_1 \\ \dot{a}_2 \\ \dot{a}_3 \\ \dot{a}_4 \end{pmatrix} = \begin{pmatrix} -\gamma/2 & 0 & 0 & -ib_{14}e^{+i(\omega_{14}-\omega)t} \\ 0 & -\gamma/2 & 0 & 0 \\ 0 & 0 & -\gamma/2 & -ib_{34}e^{+i(\omega_{34}-\omega)t} \\ -ib_{14}^{*}e^{-i(\omega_{14}-\omega)t} & 0 & -ib_{34}^{*}e^{-i(\omega_{34}-\omega)t} & -\gamma/2 \end{pmatrix} \begin{pmatrix} a_1 \\ a_2 \\ a_3 \\ a_4 \end{pmatrix} , \qquad \text{(A1)}
$$

in which,

$$b_{14} = (H_{1x} - iH_{1y})(cg_J\mu_B^e - sg_\mu'\mu_B^\mu)/(4\hbar) , \qquad \text{(A1a)}$$

$$b_{34} = -(H_{1x} + iH_{1y})(sg_J\mu_B^e - cg_\mu'\mu_B^\mu)/(4\hbar) , \qquad \text{(A1b)}$$

$$c = \tfrac{1}{2}\sqrt{2}\,[1 + x/(1+x^2)^{1/2}]^{1/2} , \qquad \text{(A1c)}$$

$$s = \tfrac{1}{2}\sqrt{2}\,[1 - x/(1+x^2)^{1/2}]^{1/2} . \qquad \text{(A1d)}$$

The other symbols have been defined in Sec. II.

We introduce the substitutions

$$a_n' = a_n e^{\gamma t/2} , \quad n = 1, 2, 3, 4 \qquad \text{(A2a)}$$

and define

$$\omega_{14}' = \omega_{14} - \omega , \quad \omega_{34}' = \omega_{34} - \omega . \qquad \text{(A2b)}$$

The differential equations for the a_n' are

$$
\begin{pmatrix} \dot{a}'_1 \\ \dot{a}'_2 \\ \dot{a}'_3 \\ \dot{a}'_4 \end{pmatrix} = \begin{pmatrix} 0 & 0 & 0 & -ib_{14}e^{+i\omega'_{14}t} \\ 0 & 0 & 0 & 0 \\ 0 & 0 & 0 & -ib_{34}e^{+i\omega'_{34}t} \\ -ib^*_{14}e^{-i\omega'_{14}t} & 0 & -ib^*_{34}e^{-i\omega'_{34}t} & 0 \end{pmatrix} \begin{pmatrix} a'_1 \\ a'_2 \\ a'_3 \\ a'_4 \end{pmatrix} .
\tag{A3}
$$

We observe that a'_2 is decoupled from the remaining state amplitudes, and hence we have a three-level problem. Further decoupling of the amplitudes leading to a two-level problem is not possible since ω_{14} and ω_{34} are not equal at nonzero magnetic field. Furthermore we do not wish to make the weak-field approximation (Sec. II B1), which is that ω'_{14} (ω'_{34}) is sufficiently large so that the term involving ω'_{14} (ω'_{34}) gives a negligible contribution to the line shape for the transition ν_{34} (ν_{14}) when averaged over a muon lifetime.

Since $\dot{a}'_1$ and $\dot{a}'_3$ are given in terms of a'_4 only, solutions for a'_1 and a'_3 are readily obtained from an expression for a'_4. By manipulation of Eq. (A3) a third-order differential equation involving only a'_4 and its derivatives is obtained:

$$
\dddot{a}'_4 = -i(\omega'_{14}+\omega'_{34})\,\ddot{a}'_4 + (\omega'_{14}\omega'_{34} - |b_{14}|^2 - |b_{34}|^2)\dot{a}'_4 \\
- i(\omega'_{14}|b_{34}|^2 + \omega'_{34}|b_{14}|^2)a'_4 .
\tag{A4}
$$

The general solution is

$$
a'_4(t) = \beta_1 e^{i\alpha_1 t} + \beta_2 e^{i\alpha_2 t} + \beta_3 e^{i\alpha_3 t} ,
\tag{A5}
$$

where the constants β_1, β_2, and β_3 are determined by the normalization condition

$$
\sum_{n=1}^{4} |a'_n(t)|^2 = 1 \quad \text{for all } t .
\tag{A6}
$$

The constants α_1, α_2, and α_3 are the three roots of the cubic equation

$$
\alpha^3 + (\omega'_{14}+\omega'_{34})\alpha^2 + (\omega'_{14}\omega'_{34} - |b_{14}|^2 - |b_{34}|^2)\alpha \\
- \omega'_{14}|b_{34}|^2 - \omega'_{34}|b_{14}|^2 = 0 .
\tag{A7}
$$

The roots to Eq. (A7) are real and can be obtained from standard formulas.[57] Expressions for a'_1, a'_2, and a'_3 are obtained by substituting a'_4 [Eq. (A5)] into Eq. (A3) and integrating from the initial time t_0 to time t:

$$
a'_1(t) = a'_1(t_0) - b_{14}\sum_{j=1}^{3}\frac{\beta_j}{(\alpha_j+\omega'_{14})}
$$
$$
\times [e^{i(\alpha_j+\omega'_{14})t} - e^{i(\alpha_j+\omega'_{14})t_0}] ,
$$
$$
a'_2(t) = a'_2(t_0) ,
$$
$$
a'_3(t) = a'_3(t_0) - b_{34}\sum_{j=1}^{3}\frac{\beta_j}{(\alpha_j+\omega'_{34})}
$$
$$
\times [e^{i(\alpha_j+\omega'_{34})t} - e^{i(\alpha_j+\omega'_{34})t_0}] .
\tag{A8}
$$

The constants β_1, β_2, and β_3 can be evaluated from Eqs. (A5), (A6), and (A8). For the application in this paper we set $t_0 = 0$ and obtain

$$
\beta_j = \frac{1}{\lambda_j}\{(\alpha_j+\omega'_{14})(\alpha_j+\omega'_{34})a_4(0)
$$
$$
- [b^*_{14}(\alpha_j+\omega'_{34})a_1(0) - b^*_{34}(\alpha_j+\omega'_{14})a_3(0)]\} ,
\tag{A9}
$$

in which

$$
\lambda_j = 3\alpha_j^2 + 2(\omega'_{14}+\omega'_{34})\alpha_j + \omega'_{14}\omega'_{34} - |b_{14}|^2 - |b_{34}|^2 ,
$$
$$
j = 1, 2, 3 .
\tag{A9a}
$$

The spin portion of the muonium wave function is given by

$$
\chi = [a_1(t)e^{-i\omega_1 t}\chi_{1,1} + a_2(t)e^{-i\omega_2 t}\chi_{1,0}
$$
$$
+ a_3(t)e^{-i\omega_3 t}\chi_{1,-1} + a_4(t)e^{-i\omega_4 t}\chi_{0,0}] ,
\tag{A10}
$$

where the spinors χ_{F,M_F} are given in Muonium I[1] and $\omega_i = W_i/\hbar$, where W_i is the energy of the state i [Eq. (2.1)]. The expectation value of the z component of the muon spin is given by

$$
P_z(t) = \langle \chi | 2I_{\mu z} | \chi \rangle
$$
$$
= |a_1(t)|^2 - |a_3(t)|^2 + (c^2 - s^2)[|a_4(t)|^2 - |a_2(t)|^2]
$$
$$
+ 2cs[a^*_2(t)a_4(t)e^{i\omega_{24}t} + a_2(t)a^*_4(t)e^{i\omega_{42}t}] .
\tag{A11}
$$

Since the cross terms in Eq. (A11) oscillate at a frequency ω_{24} which is much higher than the muon decay rate γ, their contribution to the resonance line for an observation time interval of the order of the muon mean lifetime is of order $\gamma^2/(2\pi\Delta\nu)^2$ and hence negligible. Hence $P_z(t)$ can be taken as

$$
P_z(t) = |a_1(t)|^2 - |a_3(t)|^2
$$
$$
+ (c^2 - s^2)[|a_4(t)|^2 - |a_2(t)|^2] .
\tag{A12}
$$

Using Eq. (A2a), (A5), (A8), and (A9) and manipulating algebraically we obtain

$$P_z(t) = \{ |a_1(0)|^2 - |a_3(0)|^2 + (c^2 - s^2)[|a_4(0)|^2 - |a_2(0)|^2]\} e^{-\gamma t}$$

$$+ 4e^{-\gamma t} \sum_{j=1}^{3} \frac{1}{\lambda_j \delta_j^2} ([\cos\delta_j t - 1] \{(\alpha_j + \omega_{14}')[|a_1(0)|^2 - |a_4(0)|^2] - (\alpha_j + \omega_{34}')[|a_3(0)|^2 - |a_4(0)|^2]$$

$$+ \tfrac{1}{2}(\alpha_j - \omega_{13})(\alpha_j + \omega_{14}')[a_1(0)a_4^*(0)/b_{14} + a_1^*(0)a_4(0)/b_{14}^*]$$

$$+ \tfrac{1}{2}(\alpha_j + \omega_{13})(\alpha_j + \omega_{34}')[a_3(0)a_4^*(0)/b_{34} + a_3^*(0)a_4(0)/b_{34}^*]$$

$$- \tfrac{1}{2}(\alpha_j + \omega_{14}')(\alpha_j + \omega_{34}')\xi_j[a_1(0)a_3^*(0)/(b_{14}b_{34}^*) + a_1^*(0)a_3(0)/(b_{14}^*b_{34})]/\omega_{13}\}$$

$$+ i\tfrac{1}{2}\delta_j \sin\delta_j t \{(\alpha_j + \omega_{14}')[a_1(0)a_4^*(0)/b_{14} - a_1^*(0)a_4(0)/b_{14}^*]$$

$$+ (\alpha_j + \omega_{34}')[a_3(0)a_4^*(0)/b_{34} - a_3^*(0)a_4(0)/b_{34}^*]$$

$$- (\alpha_j + \omega_{14}')(\alpha_j + \omega_{34}')[a_1(0)a_3^*(0)/(b_{14}b_{34}^*) - a_1^*(0)a_3(0)/(b_{14}^*b_{34})]\})$$

$$\times \{[\alpha_j^2 + \tfrac{1}{2}(\omega_{14}' + \omega_{34}')\alpha_j - |b_{14}|^2 - |b_{34}|^2][s^2|b_{14}|^2 - c^2|b_{34}|^2]/\omega_{13} + \tfrac{1}{2}\alpha_j[s^2|b_{14}|^2 + c^2|b_{34}|^2]\}, \quad (A13)$$

where

$$\delta_j^2 = -3\alpha_j^2 - 2(\omega_{14}' + \omega_{34}')\alpha_j + \omega_{13}^2 + 4(|b_{14}|^2 + |b_{34}|^2), \quad (A13a)$$

$$\xi_j = 2\alpha_j^2 + (\omega_{14}' + \omega_{34}')\alpha_j - 2(|b_{14}|^2 + |b_{34}|^2) - \omega_{13}^2 . \quad (A13b)$$

The density matrix as defined in Sec. II B 2 a for a nonzero magnetic field is given by

$$\rho(0) = \frac{1}{4}\begin{pmatrix} 1+P & 0 & 0 & 0 \\ 0 & 1-(c^2-s^2)P & 0 & 2csP \\ 0 & 0 & 1-P & 0 \\ 0 & 2csP & 0 & 1+(c^2-s^2)P \end{pmatrix}. \quad (A14)$$

Hence the z component of muon polarization averaged over an ensemble of muonium atoms is

$$\langle P_z(t) \rangle = P(c^4 + s^4)e^{-\gamma t} + Pe^{-\gamma t}\sum_{j=1}^{3}\frac{1}{\lambda_j \delta_j^2}(\cos\delta_j t - 1)$$

$$\times (2\alpha_j + \omega_{14}' + \omega_{34}' - (c^2 - s^2)\omega_{13})$$

$$\times [(\alpha_j^2 + \tfrac{1}{2}(\omega_{14}' + \omega_{34}')\alpha_j - |b_{14}|^2 - |b_{34}|^2)$$

$$\times (s^2|b_{14}|^2 - c^2|b_{34}|^2)/\omega_{13}$$

$$+ \tfrac{1}{2}\alpha_j(s^2|b_{14}|^2 + c^2|b_{34}|^2)]. \quad (A15)$$

The differential signal for the time interval $t_1 = 0$ to $t_2 = \infty$ is analogous to Eq. (2.27),

$$dS(\theta) = a\cos\theta\, K''L'', \quad (A16)$$

where

$$K'' = P/[1 + aP(c^4 + s^4)\cos\theta], \quad (A16a)$$

$$L'' = -\sum_{j=1}^{3}\frac{1}{\lambda_j(\delta_j^2 + \gamma^2)}[2\alpha_j + \omega_{14}' + \omega_{34}' - (c^2 - s^2)\omega_{13}]$$

$$\times \{[\alpha_j^2 + \tfrac{1}{2}(\omega_{14}' + \omega_{34}')\alpha_j - |b_{14}|^2 - |b_{34}|^2]$$

$$\times (s^2|b_{14}|^2 - c^2|b_{34}|^2)/\omega_{13}$$

$$+ \tfrac{1}{2}\alpha_j(s^2|b_{14}|^2 + c^2|b_{34}|^2)\}. \quad (A16b)$$

We have not succeeded in casting Eq. (A16b) into a readily interpretable form. However, extensive use of computer-generated line shapes has made Eq. (A16) valuable for the evaluation of resonance line shapes in a low magnetic field, as given in Tables I and II and Figs. 3 and 4.

The treatment of the muonium line shapes at nonzero magnetic field can be made somewhat more general by the introduction of the amplitudes

$$c_n(t) = a_n'(t)e^{-i\omega_n t}, \quad n = 1, 2, 3, 4. \quad (A17)$$

The time dependence of the state amplitudes $c_n(t)$ is obtained from Eqs. (A5) and (A8):

$$c_1(t) = c_1(t_0)e^{-i\omega_1(t-t_0)} - b_{14}e^{-i\omega_1 t}\sum_{j=1}^{3}\frac{\beta_j(t_0)}{(\alpha_j + \omega_{14}')}$$

$$\times [e^{i(\alpha_j + \omega_{14}')t} - e^{i(\alpha_j + \omega_{14}')t_0}],$$

$$c_2(t) = c_2(t_0)e^{-i\omega_2(t-t_0)}, \quad (A18)$$

$$c_3(t) = c_3(t_0)e^{-i\omega_3(t-t_0)} - b_{34}e^{-i\omega_3 t}\sum_{j=1}^{3}\frac{\beta_j(t_0)}{(\alpha_j + \omega_{34}')}$$

$$\times [e^{i(\alpha_j + \omega_{34}')t} - e^{i(\alpha_j + \omega_{34}')t_0}],$$

$$c_4(t) = e^{-i\omega_4 t}\sum_{j=1}^{3}\beta_j(t_0)e^{i\alpha_j t}.$$

From the normalization condition

$$\sum_{n=1}^{4}|c_n(t)|^2 = 1 \text{ for all } t, \quad (A19)$$

the constants $\beta_j(t_0)$ are given by

$$\beta_j(t_0) = (1/\lambda_j)e^{-i(\alpha_j - \omega_4)t_0}\{(\alpha_j + \omega_{14}')(\alpha_j + \omega_{34}')c_4(t_0)$$

$$- e^{i(\omega t_0 + \phi)}[b_{14}^*(\alpha_j + \omega_{34}')c_1(t_0)$$

$$- b_{34}^*(\alpha_j + \omega_{14}')c_3(t_0)]\}, \quad (A20)$$

and ϕ is the arbitrary phase of the microwave field at time t_0.

The z component of the muon polarization [see Eq. (A12)] is given by

$$P_z(t) = \{ \, |c_1(t)|^2 - |c_3(t)|^2$$

$$+ (c^2 - s^2)[\,|c_4(t)|^2 - |c_2(t)|^2]\} e^{-\gamma t} . \qquad (A21)$$

By repeated application of Eq. (A18) the time de-

velopment of the muon polarization can be obtained for muonium atoms which are introduced into a microwave field which varies in magnitude or phase, as is the case with the separated-oscillating-field method.[7]

---

†Present address: Los Alamos Scientific Laboratory, Los Alamos, N. M.
‡Present address: Physics Department, Princeton University, Princeton, N. J.
§Present address: Physics Department, Oregon State University, Corvallis, Ore.
‖Present address: University of Heidelberg, Heidelberg, Germany.
**Present address: Physics Department, University of Washington, Seattle, Wash.

[1]V. W. Hughes, D. W. McColm, K. Ziock, and R. Prepost, Phys. Rev. A **1**, 595 (1970); Phys. Rev. A **2**, 551 (1970). This paper is referred to as Muonium I.

[2]J. M. Bailey, W. E. Cleland, V. W. Hughes, R. Prepost, and K. Ziock, Phys. Rev. A **3**, 871 (1971). This paper is referred to as Muonium II.

[3]W. E. Cleland, J. M. Bailey, M. Eckhause, V. W. Hughes, R. Prepost, J. E. Rothberg, and R. M. Mobley, Phys. Rev. A **5**, 2338 (1972). This paper is referred to as Muonium III. We correct here a small misprint in Muonium III. In Eq. (4.9a) on the right-hand side, the exponent of the ($\frac{1}{2}\alpha$) term which is farthest to the right should be 4 rather than 2.

[4]V. W. Hughes, Annu. Rev. Nucl. Sci. **16**, 445 (1966).

[5]P. Kusch and V. W. Hughes, in *Encyclopedia of Physics* (Springer-Verlag, Berlin, 1959), Vol. 37/1, p. 1.

[6]C. H. Townes and A. L. Schawlow, *Microwave Spectroscopy* (McGraw-Hill, New York, 1955).

[7]D. Favart, P. M. McIntyre, D. Y. Stowell, V. L. Telegdi, R. DeVoe, and R. A. Swanson, Phys. Rev. Lett. **27**, 1336 (1971).

[8]D. Favart, P. M. McIntyre, D. Y. Stowell, V. L. Telegdi, R. DeVoe, and R. A. Swanson, Phys. Rev. Lett. **27**, 1340 (1971).

[9]P. A. Thompson, J. J. Amato, P. Crane, V. W. Hughes, R. M. Mobley, G. zu Putlitz, and J. E. Rothberg, Phys. Rev. Lett. **22**, 163 (1969); P. A. Thompson, J. J. Amato, V. W. Hughes, R. M. Mobley, and J. E. Rothberg, Bull Am. Phys. Soc. **11**, 343 (1966); and Bull. Am. Phys. Soc. **12**, 75 (1967); P. Crane, P. A. Thompson, J. J. Amato, V. W. Hughes, R. M. Mobley, G. zu Putlitz, and J. E. Rothberg, Bull. Am. Phys. Soc. **14**, 88 (1969).

[10]P. Crane, J. J. Amato, V. W. Hughes, D. M. Lazarus, G. zu Putlitz, and P. A. Thompson, in *High Energy Physics and Nuclear Structure*, edited by S. Devons (Plenum, New York, 1970), p. 677.

[11]P. A. Thompson, D. Casperson, P. Crane, T. Crane, P. Egan, V. W. Hughes, G. zu Putlitz, and R. Stambaugh, in *Proceedings of the International Conference on Precision Measurement and Fundamental Constants*, edited by D. N. Langenberg and B. N. Taylor, Natl. Bur. Stds. Publ. No. 343 (U. S. GPO, Washington, D. C., 1971), p. 339.

[12]T. Crane, D. Casperson, P. Crane, P. Egan, V. W. Hughes, R. Stambaugh, P. A. Thompson, and G. zu Putlitz, Phys. Rev.

Lett. **27**, 474 (1971).

[13]N. F. Ramsey, in *Recent Research in Molecular Beams*, edited by I. Estermann (Academic, New York, 1959), p. 107.

[14]P. A. Thompson, Ph.D. thesis (Yale University, 1967) (unpublished).

[15]P. Crane, Jr., Ph.D. thesis (Yale University, 1969) (unpublished).

[16]R. C. Tolman, *The Principles of Statistical Mechanics*, (Oxford U. P., Oxford, England, 1938).

[17]H. A. Tolhoek, Rev. Mod. Phys. **28**, 277 (1956).

[18]Manufactured by Allegheny-Ludlum Co.

[19]Manufactured by Tec Welding and Experi-Metal Co.

[20]R. A. Bernheim, *Optical Pumping* (Benjamin, New York, 1965).

[21]Manufactured by Automation-Förster Co.; model No. 5050.

[22]Research-grade gases from Linde, Inc.; O_2 content < 1 ppm.

[23]Manufactured by Whitey Research Tool Co.; model No. LC10.

[24]Manufactured by Fisher Scientific Company; model No. 15-040B.

[26]*Technique of Microwave Measurements*, edited by C. G. Montgomery (McGraw-Hill, New York, 1947).

[27]Manufactured by Hewlett-Packard Co.; model No. 5100A/5110A.

[28]Manufactured by Boonton Radio Co.; model No. 230A.

[29]Manufactured by Hewlett-Packard; model No. 33004.

[30]Manufactured by I-Tel, Inc.; model No. FBT/0.2-4500/200-4/50-28A/28A.

[31]Manufactured by Hewlett-Packard; model No. 8551B/851B

[32]Manufactured by Servo Corp. with Varian model No. 616G/TWT.

[33]Manufactured by Hewlett-Packard; model No. 431B.

[34]Manufactured by Radio Corporation of Amercia; RCA 4317.

[35]Manufactured by Digital Electronics Corporation.

[36]Manufactured by International Business Machine; model No. 727-II.

[37]J. Rosen, Nevis Report No. 92 (Columbia University, 1960) (unpublished).

[38]H. Cramer, *Mathematical Methods of Statistics* (Princeton U. P., Princeton, N. J., 1946); *The Elements of Probability Theory* (Wiley, New York, 1955); Eq. (4.2) of Muonium III had a misprint and should be the same as Eq. (4.2) of the present paper.

[39]E. S. Ensberg and C. L. Morgan, in *Proceedings of the International Conference on Precision Measurement and Fundamental Constants*, edited by D. N. Langeberg and B. N. Taylor, Natl. Bur. Stds. Spec. Publ. No. 343 (U. S. GPO, Washington, D. C., 1971), p. 321.

[40]J. J. Wright, L. C. Balling, and R. H. Lambert, Phys. Rev. A **1**,1018 (1970).

[41]W. E. Cleland, J. M. Bailey, M. Eckhouse, V. W. Hughes, R. M. Mobley, R. Prepost, and J. E. Rothberg, Phys. Rev. Lett. **13**, 202 (1964).

[42]R. DeVoe, P. M. McIntyre, A. Magnon, D. Y. Stowell, R. A. Swanson, and V. L. Telegdi, Phys. Rev. Lett. **25**, 1779 (1970).

[43]S. J. Brodsky and S. D. Drell, Annu. Rev. Nucl. Sci.

20, 147 (1970).

[44]T. Kinoshita and P. Cvitanovic, Phys. Rev. Lett. **29**, 1534 (1972).

[45]K. M. Evenson, J. S. Wells, F. R. Petersen, B. L. Danielson, G. W. Day, R. L. Barger, and J. L. Hall, Phys. Rev. Lett. **29**, 1346 (1972).

[46]B. N. Taylor, W. H. Parker, and D. N. Langenberg, Rev. Mod. Phys. **41**, 375 (1969).

[47]K. M. Crowe, J. F. Hague, J. E. Rothberg, A. Schenck, D. L. Williams, R. W. Williams, and K. K. Young, Phys. Rev. D **5**, 2145 (1972).

[48]J. Bailey, W. Bartl, G. von Bochmann, R. C. A. Brown, F. J. M. Farley, M. Giesch, H. Jöstlein, S. van der Meer, E. Picasso, and R. W. Williams, Nuovo Cimento 9A, Ser. 11, 369 (1972).

[49]J. C. Wesley and A. Rich, Phys. Rev. A **4**, 1341 (1971); S. Granger and G. W. Ford, Phys. Rev. Lett. **28**, 1479 (1972).

[50]S. J. Brodsky and G. W. Erickson, Phys. Rev. **148**, 26 (1966).

[51]V. W. Hughes, in *Physics of the One- and Two-Electron Atoms,* edited by F. Bopp and H. Kleinpoppen (North-Holland, Amsterdam, 1969), p. 407.

[52]B. E. Lautrup, A. Peterman, and E. deRafael, Phys. Rept. 3C, 193 (1972).

[53]S. Ray and S. L. Kaufman, Phys. Rev. Lett. **29**, 895 (1972).

[54]E. S. Ensberg and C. L. Morgan, Phys. Lett. 28A, 106 (1968).

[55]G. A. Clarke, J. Chem. Phys. **36**, 2211 (1962).

[56]*High-Energy Physics and Nuclear Structure,* edited by S. Devons (Plenum, New York, 1970).

[57]*Standard Mathematical Tables,* edited by S. M. Selby (Chemical Rubber Company, Cleveland, 1968).

Comparison of Two Statistical Approaches to Calculate Atomic and Molecular Orbitals*

Poul Jørgensen and Yngve Öhrn

Quantum Theory Project, Departments of Chemistry and Physics, University of Florida, Gainesville Florida 32601

(Received 26 February 1973)

The $X\alpha$ method for the calculation of atomic and molecular orbitals is compared to a method employing ensemble averages. The formal theory as well as calculated results are discussed and the choice of α parameter values for the local exhange approximation is commented upon.

I. INTRODUCTION

Comparisons are made in this paper between the $X\alpha$ method as introduced by Slater[1] or the $MSX\alpha$ method as used by Slater and Johnson[2] and the so-called grand canonical (GC) and canonical (C) Hartree-Fock (HF) methods recently applied to the calculation of atomic[3,4] and molecular[5-7] properties and spectra. This is done in an attempt to understand some of the formal aspects of the extremely simple and sometimes rather successful $X\alpha$ approach of using a local approximation to the exchange potential. (Local exchange-correlation approximations have been suggested[8] which are more accurate than the one normally used in the $X\alpha$ approximation. Studies of the nonlocal energy-dependent self-energy operator from many-body theory have produced local approximations of high accuracy, and our remarks regarding the errors in the local approximations to the exchange potential will not generally apply to these more exact treatments.) In Sec. II we give a brief outline of the different methods and in Sec. III we attempt to demonstrate that the GCHF method is a sensible method, from a formal point of view, to use as a comparison when the values of the atomic α parameters are determined. In Sec. IV we discuss the idea of the transition state as applied to the

different methods and we give some comparative results for the $X\alpha(MSX\alpha)$ method and the GCHF method as applied to the chlorine atom and the water molecule. We state our conclusions in Sec. V.

II. DESCRIPTION OF METHODS

It is demonstrated in Ref. 3 how a statistical average can be used to define an energy functional

$$\langle H \rangle = \sum_s h_{ss} \langle n_s \rangle$$

$$+ \frac{1}{2}\sum_{st} [(ss|tt) - (st|ts)] \langle n_s \rangle \langle n_t \rangle, \qquad (1)$$

in terms of an orthonormal basis of spin orbitals $[u_s(x)]$. Here h contains the one-electron terms and $(ss|tt)$ is the two-electron integral over the orbital densities $u_s^*(x_1)u_s(x_1)$ and $u_t^*(x_2)u_t(x_2)$. The average values are calculated with respect to a density operator

$$\rho = \prod_s [1 - \langle n_s \rangle + (2\langle n_s \rangle - 1)n_s], \qquad (2)$$

where n_s is the occupation number operator for spin orbital $u_s(x)$ and the average $\langle n_s \rangle$, formed with respect to ρ, is the occupation number. When these averages refer to equilibrium situations in statistical mechanics we can obtain the occupation numbers in terms of thermodynamic parameters; e.g., $\langle n_s \rangle$ will be given by the Fermi-Dirac distri-